Chapter 8

Hydrodynamics and Transport Coefficients

Chapter 7 was concerned largely with the formal definition and general properties of time correlation functions and with the link that exists between spontaneous, time-dependent fluctuations and the response of a fluid to an external probe. The main objectives of the present chapter are, first, to show how the decay of fluctuations is described within the framework of linearised hydrodynamics and, secondly, to obtain explicit expressions for the macroscopic transport coefficients in terms of microscopic quantities. The hydrodynamic approach is valid only on scales of length and time much larger than those characteristic of the molecular level, but we show how the gap between the microscopic and macroscopic descriptions can be bridged by an essentially phenomenological extrapolation of the hydrodynamic results to shorter wavelengths and higher frequencies. The same problem is taken up in a more systematic way in Chapter 9.

8.1 THERMAL FLUCTUATIONS AT LONG WAVELENGTHS AND LOW FREQUENCIES

We have seen in Section 4.1 that the microscopic structure of a liquid is revealed experimentally by the scattering of radiation of wavelength comparable with the interparticle spacing. Examination of a typical pair distribution function, such as the one pictured in Figure 2.3, shows that positional correlations decay rapidly in space and are negligibly small at separations beyond a few molecular diameters. From a static point of view, therefore, a fluid behaves, for longer wavelengths, essentially as a continuum. When discussing the dynamics, however, it is necessary to consider simultaneously the scales of both length and time. In keeping with traditional kinetic theory it is conventional to compare wavelengths with the mean free path l_c and times with the mean collision time τ_c. The wavenumber-frequency plane may then be divided into three parts. The region in which $kl_c \ll 1$, $\omega\tau_c \ll 1$ corresponds to the *hydrodynamic* regime, in which the behaviour of the fluid is described by the phenomenological equations

Theory of Simple Liquids, Fourth Edition. http://dx.doi.org/10.1016/B978-0-12-387032-2.00008-8

of macroscopic fluid mechanics. The range of intermediate wavenumbers and frequencies ($kl_c \approx 1, \omega\tau_c \approx 1$) forms the *kinetic* regime, where allowance must be made for the molecular structure of the fluid and a treatment based on the microscopic equations of motion is required. Finally, the region where $kl_c \gg 1$, $\omega\tau_c \gg 1$ represents the *free-particle* or *ballistic* regime; here the distances and times involved are so short that the particles move almost independently of each other.

In this chapter we shall be concerned mostly with the hydrodynamic regime, where the local properties of the fluid vary slowly on microscopic scales of length and time. The set of *hydrodynamic variables* or *hydrodynamic fields* include the densities of mass (or particle number), energy and momentum; these are closely related to the conserved microscopic variables introduced in Section 7.4. Like their microscopic counterparts, the conserved hydrodynamic variables satisfy continuity equations of the form (7.4.3), which express the conservation of matter, energy and momentum. In addition, there exist certain *constitutive relations* between the fluxes (or currents) and gradients of the local variables, expressed in terms of phenomenological *transport coefficients*. Fick's law of diffusion and Fourier's law of heat transport are two of the more familiar examples of a constitutive relation.

One of the main tasks of the present chapter is to obtain microscopic expressions for the transport coefficients that are similar in structure to the formula (7.7.10) already derived for the electrical conductivity of an ionic fluid. This is achieved by calculating the *hydrodynamic limit* of the appropriate time correlation function. To understand what is involved in such a calculation it is first necessary to clarify the relationship between hydrodynamic and microscopic dynamical variables. As an example, consider the local density. The microscopic particle density $\rho(\mathbf{r}, t)$ is defined by (7.4.5); its integral over all volume is equal to N, the total number of particles in the system. The hydrodynamic local density $\bar{\rho}(\mathbf{r}, t)$ is obtained by averaging the microscopic density over a sub-volume v around the point $\mathbf{r}$ that is macroscopically small but still sufficiently large to ensure that the relative fluctuations in the number of particles inside v is negligible. Then

$$\bar{\rho}(\mathbf{r}, t) = \frac{1}{v} \int_v \rho(\mathbf{r}' - \mathbf{r}, t) \mathrm{d}\mathbf{r}' \tag{8.1.1}$$

Strictly speaking, the definition of $\bar{\rho}(\mathbf{r}, t)$ also requires a smoothing or 'coarse graining' in time. This can be realised by averaging (8.1.1) over a time interval that is short on a macroscopic scale but long in comparison with the mean collision time. In practice, however, smoothing in time is already achieved by (8.1.1) if the sub-volume is sufficiently large. The Fourier components of the hydrodynamic density are defined as

$$\bar{\rho}_{\mathbf{k}}(t) = \int \bar{\rho}(\mathbf{r}, t) \exp(-i\mathbf{k} \cdot \mathbf{r}) \mathrm{d}\mathbf{r} \tag{8.1.2}$$

where the wavevector $\mathbf{k}$ must be such that k is less than about $2\pi/v^{1/3}$. The corresponding density autocorrelation function is then defined as in (7.4.20), except that the Fourier components of the microscopic density are replaced by $\bar{\rho}_{\mathbf{k}}$. Since we are now working at the macroscopic level, the average to be taken is not an ensemble average but an average over initial conditions, weighted by the probability density of thermodynamic fluctuation theory described in Appendix A. By forming such an average we are implicitly invoking the hypothesis of *local thermodynamic equilibrium*. In other words, we are assuming that although the hydrodynamic densities vary over macroscopic lengths and times, the fluid contained in each of the sub-volumes is in a state of thermodynamic equilibrium, and that the local density, pressure and temperature satisfy the usual relations of equilibrium thermodynamics. These assumptions are particularly plausible at high densities, since in that case local equilibrium is rapidly brought about by collisions between particles.

Once the calculation we have described in words has been carried out, the relations of interest are obtained by supposing that in the limit of long wavelengths ($\lambda \gg l_c$) and long times ($t \gg \tau_c$) or, equivalently, of small wavenumbers and low frequencies, correlation functions derived from the hydrodynamic equations are identical to the correlation functions of the corresponding microscopic variables. This intuitively appealing hypothesis, which is due to Onsager, can be justified on the basis of the fluctuation-dissipation theorem discussed in Section 7.6. In the example of the density autocorrelation function the assumption can be expressed by the statement that

$$\langle \rho_{\mathbf{k}}(t)\rho_{-\mathbf{k}}\rangle \sim \langle \bar{\rho}_{\mathbf{k}}(t)\bar{\rho}_{-\mathbf{k}}\rangle\,, \quad kl_c \ll 1,\ t/\tau_c \gg 1 \tag{8.1.3}$$

with the qualification, explained above, that the meaning of the angular brackets is different for the two correlation functions. Since the sections that follow are concerned almost exclusively with the calculation of correlation functions of hydrodynamic variables, no ambiguity is introduced by dropping the bar we have used to distinguish the latter from the corresponding microscopic quantities.

One important implication of the assumption of local thermodynamic equilibrium is that the Maxwell distribution of velocities applies at the local level. The local velocity $\mathbf{u}(\mathbf{r},t)$ is defined via the relation

$$\mathbf{p}(\mathbf{r},t) = \rho_m(\mathbf{r},t)\mathbf{u}(\mathbf{r},t) \tag{8.1.4}$$

where $\mathbf{p}(\mathbf{r},t)$ is the momentum density and $\rho_m(\mathbf{r},t) = m\rho(\mathbf{r},t)$ is the mass density (we assume that the fluid consists of only one component). The single-particle distribution function is now a function of $\mathbf{r}$ and t and (2.1.26) is replaced by

$$f_{\text{l.e.}}(\mathbf{u},\mathbf{r};t) = \rho(\mathbf{r},t)\left(\frac{m}{2\pi k_{\text{B}}T(\mathbf{r},t)}\right)^{3/2}\exp\left(\frac{-m|\mathbf{u}-\mathbf{u}(\mathbf{r},t)|^2}{2k_{\text{B}}T(\mathbf{r},t)}\right) \tag{8.1.5}$$

where $T(\mathbf{r},t)$ is the local temperature. The function $f_{\text{l.e.}}(\mathbf{u},\mathbf{r};t)$ is called the 'local equilibrium' Maxwell distribution.

8.2 SPACE-DEPENDENT SELF MOTION

As an illustration of the general procedure described in the previous section we first consider the relatively simple problem of the diffusion of tagged particles. If the tagged particles are physically identical to the other particles in the fluid, and if their concentration is sufficiently low that their mutual interactions can be ignored, the problem is equivalent to that of single-particle motion as described by the self part of the van Hove correlation function $G_s(\mathbf{r},t)$ (see Section 7.4). The macroscopic, tagged-particle density $\rho^{(s)}(\mathbf{r},t)$ and current $\mathbf{j}^{(s)}(\mathbf{r},t)$ satisfy a continuity equation of the form

$$\frac{\partial \rho^{(s)}(\mathbf{r},t)}{\partial t} + \nabla \cdot \mathbf{j}^{(s)}(\mathbf{r},t) = 0 \tag{8.2.1}$$

and the corresponding constitutive equation is provided by Fick's law:

$$\mathbf{j}^{(s)}(\mathbf{r},t) = -D\nabla \rho^{(s)}(\mathbf{r},t) \tag{8.2.2}$$

where the interdiffusion constant D is in this case the same as the self-diffusion constant. Combination of (8.2.1) and (8.2.2) yields the *diffusion equation*:

$$\frac{\partial \rho^{(s)}(\mathbf{r},t)}{\partial t} = D\nabla^2 \rho^{(s)}(\mathbf{r},t) \tag{8.2.3}$$

or, in reciprocal space:

$$\frac{\partial \rho_{\mathbf{k}}^{(s)}(t)}{\partial t} = -Dk^2 \rho_{\mathbf{k}}^{(s)}(t) \tag{8.2.4}$$

Equation (8.2.4) can be integrated immediately to give

$$\rho_{\mathbf{k}}^{(s)}(t) = \rho_{\mathbf{k}}^{(s)} \exp\left(-Dk^2 t\right) \tag{8.2.5}$$

where $\rho_{\mathbf{k}}^{(s)}$ is a Fourier component of the tagged-particle density at $t = 0$. If we multiply both sides of (8.2.5) by $\rho_{-\mathbf{k}}^{(s)}$ and take the thermal average, we find that the normalised autocorrelation function is

$$\frac{1}{n}\left\langle \rho_{\mathbf{k}}^{(s)}(t)\rho_{-\mathbf{k}}^{(s)}\right\rangle = \frac{1}{n}\left\langle \rho_{\mathbf{k}}^{(s)}\rho_{-\mathbf{k}}^{(s)}\right\rangle \exp\left(-Dk^2 t\right) = \exp\left(-Dk^2 t\right) \tag{8.2.6}$$

where n is the total number of tagged particles. Here we have used the fact that, because the concentration of tagged particles is low, their coordinates are mutually uncorrelated. It then follows from the general hypothesis discussed in Section 8.1 that in the hydrodynamic limit the self part of the density

autocorrelation function (7.4.21), i.e. the self-intermediate scattering function defined by (7.5.12), behaves as

$$F_s(k,t) \sim \exp\left(-Dk^2 t\right), \quad kl_c \ll 1,\ t/\tau_c \gg 1 \tag{8.2.7}$$

The long-wavelength, low-frequency limit of the van Hove self correlation function is the spatial Fourier transform of (8.2.7):

$$G_s(r,t) = \frac{1}{(4\pi Dt)^{3/2}} \exp\left(-r^2/4Dt\right) \tag{8.2.8}$$

In the same limit the self dynamic structure factor is

$$S_s(k,\omega) = \frac{1}{\pi} \frac{Dk^2}{\omega^2 + (Dk^2)^2} \tag{8.2.9}$$

Equation (8.2.9) represents a single, Lorentzian curve centred at $\omega = 0$ with a width at half-height equal to $2Dk^2$. A spectrum of this type is typical of any diffusive process described by an equation similar to (8.2.3). Alternatively, the structure of the Laplace transform of (8.2.7), i.e.

$$\tilde{F}_s(k,z) = \frac{1}{-iz + Dk^2} \tag{8.2.10}$$

shows that a diffusive process is characterised by a purely imaginary pole at $z = -iDk^2$. It should be emphasised again that the simple result expressed by (8.2.9) is valid only for $kl_c \ll 1, \omega\tau_c \ll 1$. Its breakdown at high frequencies is reflected in the fact that the even frequency moments (beyond zeroth order) of $S_s(k,\omega)$ are all infinite. Note also that the transport coefficient D is related to the behaviour of $S_s(k,\omega)$ in the limit $k, \omega \to 0$. From (8.2.9) we see that

$$D = \lim_{\omega \to 0} \lim_{k \to 0} \frac{\omega^2}{k^2} \pi S_s(k,\omega) \tag{8.2.11}$$

where it is crucial that the limits are taken in the correct order, i.e. $k \to 0$ before $\omega \to 0$. In principle, (8.2.11) provides a means of determining D from the results of inelastic scattering experiments.

Equations (7.5.16) and (8.2.8) show that the van Hove self correlation function is a gaussian function of r both for $t \to 0$ (free-particle behaviour) and $t \to \infty$ (the hydrodynamic limit); it is therefore tempting to suppose that the function is gaussian at all times. To study this point in more detail we write $G_s(r,t)$ as a generalised gaussian function of r in the form

$$G_s(r,t) = \left(\frac{\alpha(t)}{\pi}\right)^{3/2} \exp\left[-\alpha(t) r^2\right] \tag{8.2.12}$$

where $\alpha(t)$ is a function of t but not of r; the hydrodynamic limit corresponds to taking $\alpha(t) = 1/4Dt$ and the ideal-gas model to $\alpha(t) = m/2k_{\mathrm{B}}Tt^2$. The mean-square displacement of tagged particles after a time t is the second moment of $G_{\mathrm{s}}(r,t)$, i.e.

$$\left\langle r^2(t)\right\rangle \equiv \left\langle |\mathbf{r}(t) - \mathbf{r}(0)|^2 \right\rangle = \int r^2 G_{\mathrm{s}}(r,t)\mathrm{d}\mathbf{r} \tag{8.2.13}$$

and is therefore related to the unknown function $\alpha(t)$ by $\left\langle r^2(t)\right\rangle = 3/2\alpha(t)$. If we insert this result in (8.2.12) and take the Fourier transform, we find that in the gaussian approximation the self intermediate scattering function has the form

$$F_s(k,t) = \exp\left(-\frac{1}{6}k^2\left\langle r^2(t)\right\rangle\right) \tag{8.2.14}$$

Systematic corrections to the gaussian approximation can be obtained from a cumulant expansion of $F_s(k,t)$ in powers of k^2. Comparison with molecular dynamics results for argon-like liquids shows that in the intermediate range of k between the free-particle and hydrodynamic regimes the first correction (of order k^4) to (8.2.14) is typically 10% or less and positive; corrections of higher order are even smaller.[1]

The Einstein expression for the long-time limit of the mean-square displacement of a tagged particle is a direct consequence of the hydrodynamic result for $G_{\mathrm{s}}(r,t)$; substitution of (8.2.8) into the definition (8.2.13) leads immediately to (7.2.3). Since the mean-square displacement is also related to the velocity autocorrelation function through (7.2.6), there is a close connection between the functions $G_{\mathrm{s}}(r,t)$ (or $F_s(k,t)$) and $Z(t)$. In fact, in the gaussian approximation represented by (8.2.14), $F_s(k,t)$ is entirely determined by $Z(t)$ and vice versa; more generally, only the second of these statements is true. To see the significance of this connection we return briefly to the description of the system in terms of microscopic variables. If we define the Fourier components of the microscopic current associated with a tagged particle i having velocity $\mathbf{u}_i$ as

$$\mathbf{j}_{\mathbf{k}i}(t) = \mathbf{u}_i(t)\exp\left[-i\mathbf{k}\cdot\mathbf{r}_i(t)\right] \tag{8.2.15}$$

and the self-current autocorrelation function as

$$C_s(k,t) = \langle \mathbf{k}\cdot\mathbf{j}_{\mathbf{k}i}(t)\mathbf{k}\cdot\mathbf{j}_{-\mathbf{k}i}\rangle \tag{8.2.16}$$

it is clear that

$$\begin{aligned} Z(t) = \langle u_{iz}(t)u_{iz}\rangle &= \lim_{k\to 0}\frac{1}{k^2}C_s(k,t) \\ &= -\lim_{k\to 0}\frac{1}{k^2}\frac{\mathrm{d}^2}{\mathrm{d}t^2}F_s(k,t) \end{aligned} \tag{8.2.17}$$

where we have chosen $\mathbf{k}$ to lie along the z-axis and used the single-particle version of (7.4.26). The relation between the corresponding power spectra is

$$Z(\omega) = \frac{\omega^2}{2\pi} \lim_{k\to 0} \frac{1}{k^2} \int_{-\infty}^{\infty} F_s(k,t) \exp(i\omega t) \mathrm{d}t = \omega^2 \lim_{k\to 0} \frac{S_s(k,\omega)}{k^2} \tag{8.2.18}$$

Equation (8.2.18) may be regarded as a generalisation of (8.2.11) to non-zero frequencies in which $Z(\omega)$ appears as a frequency-dependent diffusion coefficient; it also provides a possible route to an experimental determination of the velocity autocorrelation function.

The relationship between $Z(t)$ and $F_s(k,t)$ (or $C_s(k,t)$) is further reflected in the short-time expansions of these functions. By analogy with (7.4.31) the expansion of $C_s(k,t)$ in powers of t can be written as

$$C_s(k,t) = \omega_0^2 \left(1 - \omega_{1s}^2 \frac{t^2}{2!} + \cdots\right) \tag{8.2.19}$$

From the general result (7.1.23) and the continuity equation (8.2.1) it follows that

$$\begin{aligned} \omega_0^2 \omega_{1s}^2 &= -\left\langle \mathbf{k}\cdot\dot{\mathbf{j}}_{\mathbf{k}i}\mathbf{k}\cdot\dot{\mathbf{j}}_{-\mathbf{k}i}\right\rangle = \langle \ddot{\rho}_{\mathbf{k}i}\ddot{\rho}_{-\mathbf{k}i}\rangle \\ &= k^4\left\langle u_{iz}^4\right\rangle + k^2\left\langle \dot{u}_{iz}^2\right\rangle = \omega_0^4 + (k^2/m^2)\left\langle F_{iz}^2\right\rangle \end{aligned} \tag{8.2.20}$$

and hence, from the definition (7.2.9), that

$$\omega_{1s}^2 = 3\omega_0^2 + \Omega_0^2 \tag{8.2.21}$$

The next term (of order t^4) in the Taylor expansion of $C_s(k,t)$ involves integrals over the triplet distribution function. Short-time expansions such as (8.2.19) are useful in extending the validity of hydrodynamic results to microscopic scales of length and time.

8.3 THE NAVIER–STOKES EQUATION AND HYDRODYNAMIC COLLECTIVE MODES

We turn now to the problem of describing the decay of long-wavelength fluctuations in the collective dynamical variables. For a one-component fluid the macroscopic local densities associated with the conserved variables are the number density $\rho(\mathbf{r},t)$, energy density $e(\mathbf{r},t)$ and momentum density $\mathbf{p}(\mathbf{r},t)$. The conservation laws for the local densities have the form

$$m\frac{\partial}{\partial t}\rho(\mathbf{r},t) + \nabla\cdot\mathbf{p}(\mathbf{r},t) = 0 \tag{8.3.1}$$

$$\frac{\partial}{\partial t}e(\mathbf{r},t) + \nabla\cdot\mathbf{J}^e(\mathbf{r},t) = 0 \tag{8.3.2}$$

$$\frac{\partial}{\partial t}\mathbf{p}(\mathbf{r},t) + \nabla \cdot \mathbf{\Pi}(\mathbf{r},t) = 0 \tag{8.3.3}$$

where $\mathbf{J}^e$ is the energy current and $\mathbf{\Pi}$ is the momentum current or *stress tensor*. These equations must be supplemented by two constitutive relations in which $\mathbf{J}^e$ and $\mathbf{\Pi}$ are expressed in terms of quantities representing dissipative processes in the fluid. We choose a frame of reference in which the mean velocity of the fluid is zero, i.e. $\langle \mathbf{u}(\mathbf{r},t)\rangle = 0$, and assume that the local deviations of the hydrodynamic variables from their average values are small. The equations may then be linearised with respect to the deviations. We consider in turn each of the three conservation laws.

Conservation of particle number. Equation (8.3.1) is easily dealt with. The assumption that the local deviation in number density is small means that the momentum density can be written as

$$\mathbf{p}(\mathbf{r},t) = m\left[\rho + \delta\rho(\mathbf{r},t)\right]\mathbf{u}(\mathbf{r},t) \approx m\rho\mathbf{u}(\mathbf{r},t) \equiv m\mathbf{j}(\mathbf{r},t) \tag{8.3.4}$$

which also serves as the definition of the local particle current $\mathbf{j}(\mathbf{r},t)$. With this approximation, (8.3.1) becomes

$$\frac{\partial}{\partial t}\delta\rho(\mathbf{r},t) + \nabla \cdot \mathbf{j}(\mathbf{r},t) = 0 \tag{8.3.5}$$

Conservation of energy. The macroscopic energy current $\mathbf{J}^e$ is defined as

$$\mathbf{J}^e(\mathbf{r},t) = (e+P)\mathbf{u}(\mathbf{r},t) - \lambda\nabla T(\mathbf{r},t) \tag{8.3.6}$$

where $e = U/V$ is the equilibrium energy density, P is the fixed, overall pressure, $e+P$ is the enthalpy density, λ is the thermal conductivity and $T(\mathbf{r},t)$ is the local temperature already introduced in (8.1.5); terms corresponding to viscous heating have been omitted, since these are quadratic in the local velocity. Equations (8.3.2), (8.3.5) and (8.3.6) can now be combined to give the *energy equation*, i.e.

$$\frac{\partial}{\partial t}\delta q(\mathbf{r},t) - \lambda\nabla^2\delta T(\mathbf{r},t) = 0 \tag{8.3.7}$$

where $\delta q(\mathbf{r},t)$ is the fluctuation in a quantity

$$q(\mathbf{r},t) = e(\mathbf{r},t) - \left(\frac{e+P}{\rho}\right)\rho(\mathbf{r},t) \tag{8.3.8}$$

which can be interpreted as a density of heat energy. If the number of particles is held constant, the entropy change of the system in an infinitesimal process is $T\,\mathrm{d}S = \mathrm{d}U + P\,\mathrm{d}V$. Hence

$$T\,\mathrm{d}S = \mathrm{d}(eV) + P\,\mathrm{d}V = V\,\mathrm{d}e - \frac{eV}{\rho}\,\mathrm{d}\rho - \frac{PV}{\rho}\,\mathrm{d}\rho = V\,\mathrm{d}q \tag{8.3.9}$$

A change in q is therefore equal to the heat lost or gained by the system per unit volume when the change is carried out reversibly and $\delta q(\mathbf{r},t)$ is related to the change in entropy density $s(\mathbf{r},t)$ by

$$\delta q(\mathbf{r},t) = T\delta s(\mathbf{r},t) \tag{8.3.10}$$

If we invoke the hypothesis of local thermodynamic equilibrium the deviation of a local thermodynamic variable such as $s(\mathbf{r},t)$ from its average value can be expressed in terms of a set of statistically independent quantities. We choose as independent variables the density and temperature (see Appendix A) and expand $q(\mathbf{r},t)$ to first order in the deviations $\delta\rho(\mathbf{r},t)$ and $\delta T(\mathbf{r},t)$. Then, from (8.3.10), and remembering that N is fixed:

$$\begin{aligned}\delta q(\mathbf{r},t) &= \frac{T}{V}\left(\frac{\partial S}{\partial \rho}\right)_T \delta\rho(\mathbf{r},t) + \frac{T}{V}\left(\frac{\partial S}{\partial T}\right)_\rho \delta T(\mathbf{r},t) \\ &= -\frac{T\beta_V}{\rho}\delta\rho(\mathbf{r},t) + \rho c_V \delta T(\mathbf{r},t) \end{aligned} \tag{8.3.11}$$

where

$$\beta_V = \left(\frac{\partial P}{\partial T}\right)_\rho = -\rho\left(\frac{\partial (S/V)}{\partial \rho}\right)_T \tag{8.3.12}$$

is the thermal pressure coefficient, c_V is the heat capacity per particle at constant volume and use has been made of the Maxwell relation $(\partial S/\partial V)_T = (\partial P/\partial T)_V$ resulting from (2.3.8). If we now substitute (8.3.11) in (8.3.7), eliminate $(\partial/\partial t)\rho(\mathbf{r},t)$ with the help of (8.3.5) and divide through by ρc_V, the energy equation becomes

$$\left(\frac{\partial}{\partial t} - a\nabla^2\right)\delta T(\mathbf{r},t) + \frac{T\beta_V}{\rho^2 c_V}\boldsymbol{\nabla}\cdot\mathbf{j}(\mathbf{r},t) = 0 \tag{8.3.13}$$

where

$$a = \frac{\lambda}{\rho c_V} \tag{8.3.14}$$

Conservation of momentum. The components of the stress tensor $\boldsymbol{\Pi}$ in (8.3.3) are given macroscopically by

$$\begin{aligned}\Pi^{\alpha\beta}(\mathbf{r},t) &= \delta_{\alpha\beta}P(\mathbf{r},t) - \eta\left(\frac{\partial u_\alpha(\mathbf{r},t)}{\partial r_\beta} + \frac{\partial u_\beta(\mathbf{r},t)}{\partial r_\alpha}\right) \\ &\quad + \delta_{\alpha\beta}\left(\frac{2}{3}\eta - \zeta\right)\boldsymbol{\nabla}\cdot\mathbf{u}(\mathbf{r},t)\end{aligned} \tag{8.3.15}$$

where $P(\mathbf{r},t)$ is the local pressure, η is the shear viscosity, ζ is the bulk viscosity and the bracketed quantity in the second term on the right-hand side is the rate-of-strain tensor.[2] Substitution of (8.3.15) in (8.3.3) and use of (8.3.5) leads to the Navier–Stokes equation in its linearised form:

$$\frac{\partial}{\partial t}\mathbf{j}(\mathbf{r},t) + \frac{1}{m}\boldsymbol{\nabla}P(\mathbf{r},t) - \nu\nabla^2\mathbf{j}(\mathbf{r},t) - \frac{\frac{1}{3}\eta + \zeta}{\rho m}\boldsymbol{\nabla}\boldsymbol{\nabla}\cdot\mathbf{j}(\mathbf{r},t) = 0 \tag{8.3.16}$$

where

$$\nu = \frac{\eta}{\rho m} \tag{8.3.17}$$

is the kinematic shear viscosity. To first order in $\delta\rho(\mathbf{r},t)$ and $\delta T(\mathbf{r},t)$ the fluctuation in local pressure is

$$\begin{aligned}\delta P(\mathbf{r},t) &= \left(\frac{\partial P}{\partial \rho}\right)_T \delta\rho(\mathbf{r},t) + \left(\frac{\partial P}{\partial T}\right)_\rho \delta T(\mathbf{r},t) \\ &= \frac{1}{\rho\chi_T}\delta\rho(\mathbf{r},t) + \beta_V \delta T(\mathbf{r},t)\end{aligned} \tag{8.3.18}$$

where χ_T is the isothermal compressibility (2.4.16). The Navier–Stokes equation can therefore be rewritten as

$$\frac{1}{\rho m \chi_T}\nabla\delta\rho(\mathbf{r},t) + \frac{\beta_V}{m}\nabla\delta T(\mathbf{r},t) + \left(\frac{\partial}{\partial t} - \nu\nabla^2 - \frac{\frac{1}{3}\eta+\zeta}{\rho m}\nabla\nabla\cdot\right)\mathbf{j}(\mathbf{r},t) = 0 \tag{8.3.19}$$

Equations (8.3.5), (8.3.13) and (8.3.19) form a closed set of linear equations for the variables $\delta\rho(\mathbf{r},t), \delta T(\mathbf{r},t)$ and $\mathbf{j}(\mathbf{r},t)$. These are readily solved by taking the double transforms with respect to space (Fourier) and time (Laplace) to give

$$-iz\tilde{\rho}_{\mathbf{k}}(z) + i\mathbf{k}\cdot\tilde{\mathbf{j}}_{\mathbf{k}}(z) = \rho_{\mathbf{k}} \tag{8.3.20}$$

$$(-iz + ak^2)\tilde{T}_{\mathbf{k}}(z) + \frac{T\beta_V}{\rho^2 c_V} i\mathbf{k}\cdot\tilde{\mathbf{j}}_{\mathbf{k}}(z) = T_{\mathbf{k}} \tag{8.3.21}$$

$$\frac{1}{\rho m\chi_T} i\mathbf{k}\tilde{\rho}_{\mathbf{k}}(z) + \frac{\beta_V}{m} i\mathbf{k}\tilde{T}_{\mathbf{k}}(z) + \left(-iz + \nu k^2 + \frac{\frac{1}{3}\eta+\zeta}{\rho m}\mathbf{k}\mathbf{k}\cdot\right)\tilde{\mathbf{j}}_{\mathbf{k}}(z) = \mathbf{j}_{\mathbf{k}} \tag{8.3.22}$$

where, for example:

$$\tilde{\rho}_{\mathbf{k}}(z) = \int_0^\infty \mathrm{d}t \exp(izt) \int \delta\rho(\mathbf{r},t)\exp(-i\mathbf{k}\cdot\mathbf{r})\mathrm{d}\mathbf{r} \tag{8.3.23}$$

and $\rho_{\mathbf{k}}$, $T_{\mathbf{k}}$ and $\mathbf{j}_{\mathbf{k}}$ are the spatial Fourier components at $t = 0$. We now separate the components of the current $\mathbf{j}_{\mathbf{k}}$ into their longitudinal and transverse parts. Taking $\mathbf{k}$ along the z-axis, we rewrite (8.3.22) as

$$\begin{aligned}&\frac{1}{\rho m\chi_T} ik\tilde{\rho}_{\mathbf{k}}(z) + \frac{\beta_V}{m} ik\tilde{T}_{\mathbf{k}}(z) + \left(-iz + bk^2\right)\tilde{j}^z_{\mathbf{k}}(z) = j^z_{\mathbf{k}} \\ &\left(-iz + \nu k^2\right)\tilde{j}^\alpha_{\mathbf{k}} = j^\alpha_{\mathbf{k}}, \quad \alpha = x, y\end{aligned} \tag{8.3.24}$$

where

$$b = \frac{\frac{4}{3}\eta+\zeta}{\rho m} \tag{8.3.25}$$

is the kinematic longitudinal viscosity.

Equations (8.3.20), (8.3.21) and (8.3.24) are conveniently summarised in matrix form:

$$\begin{pmatrix} -iz & 0 & ik & 0 & 0 \\ 0 & -iz+ak^2 & \frac{T\beta_V ik}{\rho^2 c_V} & 0 & 0 \\ \frac{ik}{\rho m \chi_T} & \frac{\beta_V ik}{m} & -iz+bk^2 & 0 & 0 \\ 0 & 0 & 0 & -iz+\nu k^2 & 0 \\ 0 & 0 & 0 & 0 & -iz+\nu k^2 \end{pmatrix} \begin{pmatrix} \tilde{\rho}_{\mathbf{k}}(z) \\ \tilde{T}_{\mathbf{k}}(z) \\ \tilde{j}^z_{\mathbf{k}}(z) \\ \tilde{j}^x_{\mathbf{k}}(z) \\ \tilde{j}^y_{\mathbf{k}}(z) \end{pmatrix} = \begin{pmatrix} \rho_{\mathbf{k}} \\ T_{\mathbf{k}} \\ j^z_{\mathbf{k}} \\ j^x_{\mathbf{k}} \\ j^y_{\mathbf{k}} \end{pmatrix} \tag{8.3.26}$$

The matrix of coefficients in (8.3.26) is called the *hydrodynamic matrix*. Its block diagonal structure shows that the transverse current fluctuations are completely decoupled from fluctuations in the other, longitudinal variables. The determinant of the hydrodynamic matrix therefore factorises into the product of purely longitudinal (l) and purely transverse (t) parts, i.e.

$$D(k,z) = D_l(k,z)D_t(k,z) \tag{8.3.27}$$

with

$$\begin{aligned} D_l(k,z) = &-iz\left(-iz+ak^2\right)\left(-iz+bk^2\right) \\ &+\left(-iz+ak^2\right)\frac{k^2}{\rho m \chi_T} - iz\frac{T\beta_V^2 k^2}{\rho^2 m c_V} \end{aligned} \tag{8.3.28}$$

and

$$D_t(k,z) = \left(-iz+\nu k^2\right)^2 \tag{8.3.29}$$

The dependence of frequency on wavenumber or *dispersion relation* for the collective modes is determined by the poles of the inverse of the hydrodynamic matrix and hence by the complex roots of the equation

$$D(k,z) = 0 \tag{8.3.30}$$

The factorisation in (8.3.27) shows that (8.3.30) has a double root associated with the two transverse modes, namely

$$z = -i\nu k^2 \tag{8.3.31}$$

while the complex frequencies corresponding to longitudinal modes are obtained as the solution to the cubic equation

$$iz^3 - z^2(a+b)k^2 - iz\left(abk^2 + c_s^2\right)k^2 + \frac{ac_s^2}{\gamma}k^4 = 0 \tag{8.3.32}$$

where $\gamma = c_P/c_V$ is the ratio of specific heats, c_s is the adiabatic speed of sound, given by

$$c_s^2 = \frac{\gamma}{\rho m \chi_T} \tag{8.3.33}$$

and use has been made of the thermodynamic relation[3]

$$c_P = c_V + \frac{T\chi_T\beta_V^2}{\rho} \tag{8.3.34}$$

Since the hydrodynamic calculation is valid only in the long-wavelength limit, it is sufficient to calculate the complex frequencies to order k^2. The algebra is simplified by introducing the reduced variables $s = z/c_s k$; it is then straightforward to show[4] that the approximate solution to (8.3.32) is

$$z_0 = -iD_T k^2, \quad z_\pm = \pm c_s k - i\Gamma k^2 \tag{8.3.35}$$

where

$$D_T = \frac{a}{\gamma} = \frac{\lambda}{\rho c_P} \tag{8.3.36}$$

is the thermal diffusivity and

$$\Gamma = \frac{a(\gamma - 1)}{2\gamma} + \frac{1}{2}b \tag{8.3.37}$$

is the sound attenuation coefficient. The imaginary roots in (8.3.31) and (8.3.35) represent diffusive processes of the type already discussed in the preceding section whereas the pair of complex roots in (8.3.35) correspond to propagating sound waves, as we shall see in Section 8.5.

8.4 TRANSVERSE CURRENT CORRELATIONS

The second relation in (8.3.24) shows that in the time domain the hydrodynamic behaviour of the transverse current fluctuations is described by a first-order differential equation of the form

$$\frac{\partial}{\partial t} j_{\mathbf{k}}^x(t) = -\nu k^2 j_{\mathbf{k}}^x(t) \tag{8.4.1}$$

This result has precisely the same structure as the diffusion equation (8.2.4) and the kinematic shear viscosity has the same dimensions as the self-diffusion coefficient, but is typically two orders of magnitude larger than D for, say, an argon-like liquid near its triple point. If we multiply through (8.4.1) by $j_{-\mathbf{k}}^x$ and take the thermal average we find that the transverse current autocorrelation function satisfies the equation

$$\frac{\partial}{\partial t} C_t(k,t) + \nu k^2 C_t(k,t) = 0 \tag{8.4.2}$$

the solution to which is

$$C_t(k,t) = C_t(k,0)\exp\left(-\nu k^2 t\right) = \omega_0^2 \exp\left(-\nu k^2 t\right) \tag{8.4.3}$$

where ω_0 is the frequency defined by (7.4.29). The exponential decay in (8.4.3) is typical of a diffusive process (see Section 8.2).

The diffusive behaviour of the hydrodynamic 'shear' mode is also apparent in the fact that the Laplace transform of $C_t(k,t)$ has a purely imaginary pole corresponding to the root (8.3.31) of $D(k,z)$:

$$\tilde{C}_t(k,z) = \frac{\omega_0^2}{-iz + \nu k^2} \tag{8.4.4}$$

Let $z = \omega + i\epsilon$ approach the real axis from above ($\epsilon \to 0+$). Then $\tilde{C}_t(k,\omega)$ at small k is given approximately by

$$\tilde{C}_t(k,\omega) = \frac{\omega_0^2}{-i\omega}\left(1 - \frac{\nu k^2}{i\omega}\right)^{-1} \approx \frac{\omega_0^2}{-i\omega}\left(1 + \frac{\nu k^2}{i\omega}\right) \tag{8.4.5}$$

If we substitute for ω_0^2 and recall the definition (8.3.17) of ν we find that the shear viscosity, which must be real, is related to the long-wavelength, low-frequency behaviour of $\tilde{C}_t(k,\omega)$ by

$$\begin{aligned}\eta &= \beta\rho m^2 \lim_{\omega\to 0}\lim_{k\to 0}\frac{\omega^2}{k^4}\mathrm{Re}\tilde{C}_t(k,\omega) \\ &= \pi\beta\rho m^2 \lim_{\omega\to 0}\lim_{k\to 0}\frac{\omega^2}{k^4}C_t(k,\omega)\end{aligned} \tag{8.4.6}$$

where $C_t(k,\omega)$ is the spectrum of transverse current fluctuations, i.e. the Fourier transform of $C_t(k,t)$; this result is the analogue of the expression for the self-diffusion coefficient given by (8.2.11). From the properties of the Laplace transform and the definition of $C_t(k,t)$ it follows that

$$\begin{aligned}\frac{k^2}{N}\int_0^\infty \left\langle \dot{j}^x_{\mathbf{k}}(t)\dot{j}^x_{-\mathbf{k}}\right\rangle \exp(i\omega t)\mathrm{d}t &= -\int_0^\infty \frac{\mathrm{d}^2}{\mathrm{d}t^2}C_t(k,t)\exp(i\omega t)\mathrm{d}t \\ &= \omega^2\tilde{C}_t(k,\omega) - i\omega\omega_0^2\end{aligned} \tag{8.4.7}$$

We may therefore rewrite (8.4.6) as

$$\eta = \frac{\beta m^2}{V}\lim_{\omega\to 0}\lim_{k\to 0}\mathrm{Re}\int_0^\infty \frac{1}{k^2}\left\langle \dot{j}^x_{\mathbf{k}}(t)\dot{j}^x_{-\mathbf{k}}\right\rangle \exp(i\omega t)\mathrm{d}t \tag{8.4.8}$$

The time derivative of the transverse current can be expressed in terms of the stress tensor via the conservation law (8.3.3). Taking the Fourier transform of (8.3.3), and remembering that $\mathbf{k}$ lies along the z-axis and $\mathbf{p}(\mathbf{r},t) = m\mathbf{j}(\mathbf{r},t)$, we find that

$$\frac{\partial}{\partial t}j^x_{\mathbf{k}}(t) + \frac{ik}{m}\Pi^{xz}_{\mathbf{k}}(t) = 0 \tag{8.4.9}$$

Combination of (8.4.8) and (8.4.9) shows that the shear viscosity is proportional to the time integral of the autocorrelation function of an off-diagonal element of the stress tensor taken in the limit $k \to 0$:

$$\eta = \frac{\beta}{V}\int_0^\infty \left\langle \Pi^{xz}_0(t)\Pi^{xz}_0\right\rangle \mathrm{d}t \equiv \int_0^\infty \eta(t)\mathrm{d}t \tag{8.4.10}$$

In order to relate the shear viscosity to the intermolecular forces it is necessary to have a microscopic expression for the stress tensor. It follows from the definition (7.4.7) of the microscopic particle current that

$$m\frac{\partial}{\partial t}j_{\mathbf{k}}^{\alpha} = m\sum_{i=1}^{N}\left(\dot{u}_{i\alpha} - \sum_{\beta} ik_{\beta}u_{i\alpha}u_{i\beta}\right)\exp\left(-i\mathbf{k}\cdot\mathbf{r}_i\right) \tag{8.4.11}$$

where α, β denote any of x, y or z; the relation to the stress tensor is then established by use of (8.4.9), with $\alpha = x$ and $\beta = z$. To introduce the pair potential $v(r)$ we note that $\mathbf{r}_{ji} = -\mathbf{r}_{ij}$, and rewrite the first term on the right-hand side of (8.4.11) successively as

$$\begin{aligned} m\sum_{i=1}^{N}\dot{u}_{i\alpha}\exp\left(-i\mathbf{k}\cdot\mathbf{r}_i\right) &= \sum_{i=1}^{N}\sum_{j\neq i}^{N}\frac{r_{ij\alpha}}{|\mathbf{r}_{ij}|}v'(r_{ij})\exp\left(-i\mathbf{k}\cdot\mathbf{r}_i\right) \\ &= \frac{1}{2}\sum_{i=1}^{N}\sum_{j\neq i}^{N}\frac{r_{ij\alpha}}{|\mathbf{r}_{ij}|}v'(r_{ij})\left[\exp\left(-i\mathbf{k}\cdot\mathbf{r}_i\right) - \exp\left(-i\mathbf{k}\cdot\mathbf{r}_j\right)\right] \\ &= \frac{1}{2}ik_{\beta}\sum_{i=1}^{N}\sum_{j\neq i}^{N}\frac{r_{ij\alpha}r_{ij\beta}}{ik_{\beta}r_{ij\beta}|\mathbf{r}_{ij}|}v'(r_{ij})\left[\exp\left(-i\mathbf{k}\cdot\mathbf{r}_i\right) - \exp\left(-i\mathbf{k}\cdot\mathbf{r}_j\right)\right] \end{aligned} \tag{8.4.12}$$

where $v'(r) \equiv \mathrm{d}v(r)/\mathrm{d}r$; the second step is taken by writing each term in the double sum as half the sum of two equal terms. On introducing a quantity $\Phi_{\mathbf{k}}(\mathbf{r})$ defined as

$$\Phi_{\mathbf{k}}(\mathbf{r}) = rv'(r)\left(\frac{\exp\left(i\mathbf{k}\cdot\mathbf{r}\right) - 1}{i\mathbf{k}\cdot\mathbf{r}}\right) \tag{8.4.13}$$

we finally obtain a microscopic expression for $\Pi_{\mathbf{k}}^{\alpha\beta}$ in the form

$$\Pi_{\mathbf{k}}^{\alpha\beta} = \sum_{i=1}^{N}\left(mu_{i\alpha}u_{i\beta} + \frac{1}{2}\sum_{j\neq i}^{N}\frac{r_{ij\alpha}r_{ij\beta}}{r_{ij}^2}\Phi_{\mathbf{k}}(\mathbf{r}_{ij})\right)\exp\left(-i\mathbf{k}\cdot\mathbf{r}_i\right) \tag{8.4.14}$$

The Green–Kubo relation for the shear viscosity analogous to (7.2.7) is then obtained by inserting (8.4.14) (taken for $\mathbf{k} = 0$) in (8.4.10). Note that it follows from the virial theorem that

$$\left\langle \Pi_0^{\alpha\alpha}\right\rangle = PV \tag{8.4.15}$$

whereas

$$\left\langle \Pi_0^{\alpha\beta}\right\rangle = 0, \quad \alpha \neq \beta \tag{8.4.16}$$

Equation (8.4.10) is not directly applicable to the hard-sphere fluid because the pair potential has a singularity at $r = d$ (the hard-sphere diameter). However,

the microscopic expression for the shear viscosity, together with formulae to be derived later for other transport coefficients, can be recast in a form that resembles the Einstein relation (7.2.3) for the self-diffusion coefficient and is valid even for hard spheres. A Green–Kubo formula for a transport coefficient K, including both (7.7.10) (taken for $\omega = 0$) and (8.4.10), can always be written as

$$K = \frac{\beta}{V}\int_0^\infty \langle \dot{A}(t)\dot{A}\rangle \, \mathrm{d}t \tag{8.4.17}$$

where A is some microscopic dynamical variable. The argument used to derive (7.2.7) from (7.2.3) can be extended to show that (8.4.17) is equivalent to writing

$$K = \frac{\beta}{V}\lim_{t\to\infty}\frac{1}{2t}\left\langle |A(t) - A(0)|^2 \right\rangle \tag{8.4.18}$$

which may be regarded as a generalised form of the Einstein relation for D. In the case of the shear viscosity we see from (8.4.8) that the variable $A(t)$ is

$$\begin{aligned} A(t) &= \lim_{k\to 0}\frac{im}{k} j^x_{\mathbf{k}}(t) \\ &= \lim_{k\to 0}\frac{im}{k}\sum_{i=1}^{N} u_{ix}(t)\left[1 - ikr_{iz}(t) + \cdots\right] = m\sum_{i=1}^{N} u_{ix}(t)r_{iz}(t) \end{aligned} \tag{8.4.19}$$

where a frame of reference has been chosen in which the total momentum of the particles (a conserved quantity) is zero. Hence the generalised Einstein relation for the shear viscosity is

$$\eta = \frac{\beta m^2}{V}\lim_{t\to\infty}\frac{1}{2t}\left\langle \left| \sum_{i=1}^{N}\left[u_{ix}(t)r_{iz}(t) - u_{ix}(0)r_{iz}(0)\right]\right|^2 \right\rangle \tag{8.4.20}$$

The quantity Π_0^{xz} in the Green–Kubo formula (8.4.10) is the sum of a kinetic and a potential term. There are consequently three distinct contributions to the shear viscosity: a purely kinetic term, corresponding to the transport of transverse momentum via the displacement of particles; a purely potential term, arising from the action of the interparticle forces ('collisional' transport); and a cross term. At liquid densities the potential term is much the largest of the three. In Enskog's theory (see Section 7.2) the shear viscosity of the hard-sphere fluid is

$$\frac{\eta_{\mathrm{E}}}{\eta_0} = \frac{2\pi\rho d^3}{3}\left(\frac{1}{y} + 0.8 + 0.761y\right) \tag{8.4.21}$$

where $y = \beta P/\rho - 1 = (2\pi\rho d^3/3)g(d)$ and $\eta_0 = (5/16d^2)(mk_{\mathrm{B}}T/\pi)^{1/2}$ is the limiting, low-density result derived from the Boltzmann equation.[5] The three terms between brackets in (8.4.21) represent, successively, the kinetic,

cross and potential contributions; the last of these is dominant close to the fluid-solid transition, where $g(d)$ (the pair distribution function at contact) ≈ 6 and $y \approx 11$. Note that the kinetic contribution scales with $g(d)$ in the same way as the diffusion constant (see Section 2.5); this is not surprising, since diffusion is a purely kinetic phenomenon.

Results obtained by molecular dynamics calculations for the self-diffusion constant and shear viscosity of the hard-sphere fluid are plotted as functions of density in Figure 8.1; the two transport coefficients are plotted in a reduced form that corresponds to setting $d = m = k_B T = 1$. A comparison between simulation and the predictions of Enskog theory was made earlier in Figure 7.3. In the case of the shear viscosity agreement is very good for densities up to $\rho d^3 \approx 0.7$. Near solidification, however, where η increases rapidly with density, the theory underestimates the shear viscosity by a factor of approximately two. The behaviour of the self-diffusion constant at high densities is the reverse of this. An inverse relationship between D and η is implicit in the Stokes–Einstein relation (7.3.19), which can be rewritten in reduced form as

$$\frac{1}{\pi D^* \eta^*} = \alpha \tag{8.4.22}$$

where $\alpha = 2$ or 3 for slip or stick boundary conditions, respectively. Figure 8.2 shows a plot of the quantity $1/\pi D^* \eta^*$ versus density in which the appearance of a plateau region extending from $\rho d^3 \approx 0.25$ up to $\rho d^3 \approx 0.9$ implies that the Stokes-Einstein relation is to a good approximation satisfied over a density range in which both D and η change by an order of magnitude but in opposite senses; the level of the plateau is close to that corresponding to slip boundary

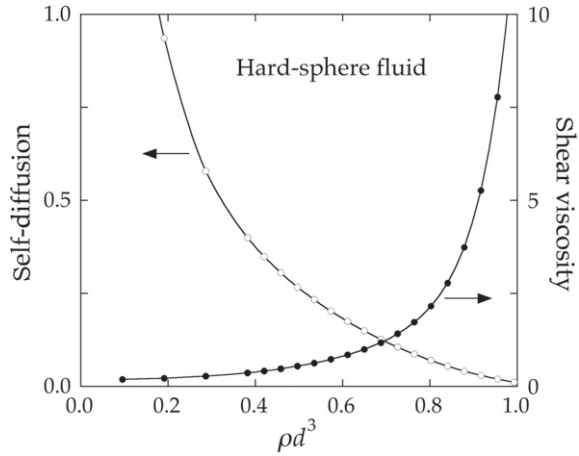

FIGURE 8.1 Variation with density of the self-diffusion coefficient and shear viscosity of the hard-sphere fluid, plotted in reduced units for which $d = m = k_B T = 1$. The points show the results of molecular dynamics calculations[6] and the curves are guides to the eye.

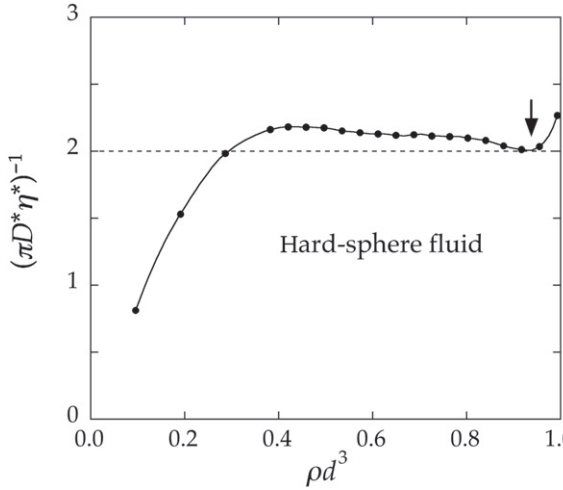

FIGURE 8.2 Test of the applicability of the Stokes–Einstein relation to the hard-sphere fluid. The points are calculated from the values of D and η shown in Figure 8.1 and the curve is a guide to the eye. The plateau in the results defines a region over which the relation is to a good approximation satisfied, with a value of α in (8.4.22) close to that corresponding to slip boundary conditions. The arrow marks the density at which the fluid–solid transition occurs. After Heyes et al.[7]

condition. No such plateau is seen in the curve computed from the Enskog values of D and η. Over the same range of density an even better fit[7] to the molecular dynamics data is provided by a 'fractional' Stokes–Einstein relation[8] of the form $D \propto (1/\eta)^{\gamma}$ with $\gamma \approx 0.975$. The same expression, with system-dependent values of $\gamma \approx 0.8$–1.0, has been used successfully in the correlation of transport data for a wide variety of liquids, but the justification for its use remains purely empirical.

The increase in shear viscosity at high densities is linked numerically to the appearance of a slowly decaying, quasi-exponential tail in the stress tensor autocorrelation function $\eta(t)$ defined by (8.4.10), colloquially called the 'molasses' tail.[9] The effect is not peculiar to hard spheres. For example, a persisting, positive tail is clearly present in the results shown in Figure 8.3 for a soft-sphere (r^{-12}) fluid at a high value of the coupling constant Γ, where $\eta(t)$ is well represented by the sum of two exponentials. At lower values of Γ, corresponding to lower densities or higher temperatures, the tail in $\eta(t)$ is barely perceptible even on a logarithmic scale.

8.5 LONGITUDINAL COLLECTIVE MODES

The longitudinal collective modes are those associated with fluctuations in density, temperature and the projection of the particle current along the direction of the wavevector **k**. It is clear from the structure of the hydrodynamic matrix

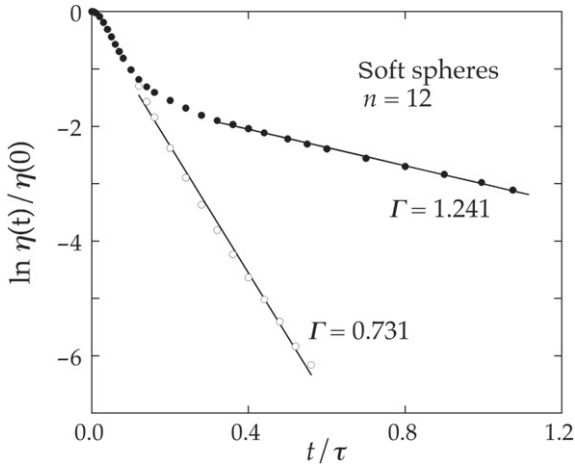

FIGURE 8.3 Normalised stress tensor autocorrelation function of a soft-sphere (r^{-12}) fluid at two values of the coupling parameter Γ defined by (5.4.13). The unit of time is $\tau = (\sigma^2/48\epsilon)^{1/2}$. Unpublished results of D.M. Heyes.

in (8.3.26) that the variables $\tilde{\rho}_{\mathbf{k}}(z)$, $\tilde{T}_{\mathbf{k}}(z)$ and $\tilde{j}^z_{\mathbf{k}}(z)$ are coupled to each other. The analysis is therefore more complicated than in the case of the transverse current fluctuations. There are three longitudinal modes, corresponding to the roots z_0, z_+ and z_- displayed in (8.3.35). The significance of the different roots is most easily grasped by solving the system of coupled, longitudinal equations represented by (8.3.26) to obtain the hydrodynamic limiting form of the dynamic structure factor $S(k,\omega)$. The solution for $\tilde{\rho}_{\mathbf{k}}(z)$ involves terms proportional to the initial values $\rho_{\mathbf{k}}, T_{\mathbf{k}}$ and $j^z_{\mathbf{k}}$. We may omit the term proportional to $j^z_{\mathbf{k}}$ because $\mathbf{k}$ can always be chosen to make $\mathbf{u}_{\mathbf{k}}$ (the Fourier transform of the initial local velocity $\mathbf{u}(\mathbf{r},0)$) perpendicular to $\mathbf{k}$, thereby ensuring that $j^z_{\mathbf{k}} = 0$. We can also ignore the term proportional to $T_{\mathbf{k}}$; this contributes nothing to the final expression for $S(k,\omega)$, since fluctuations in temperature and density are instantaneously uncorrelated, i.e. $\langle T_{\mathbf{k}}\rho_{-\mathbf{k}}\rangle = 0$ (see Appendix A). With these simplifications the solution for $\tilde{\rho}_{\mathbf{k}}(z)$ is

$$\frac{\tilde{\rho}_{\mathbf{k}}(z)}{\rho_{\mathbf{k}}} = \frac{(-iz + ak^2)(-iz + bk^2) + (\gamma - 1)c_s^2 k^2/\gamma}{D_l(k,z)} \tag{8.5.1}$$

where all quantities are as defined in Section 8.3. Separation of the right-hand side of (8.5.1) into partial fractions shows that on the real axis $\tilde{\rho}_{\mathbf{k}}$ is given by

$$\frac{\tilde{\rho}_{\mathbf{k}}(\omega)}{\rho_{\mathbf{k}}} = \left(\frac{\gamma - 1}{\gamma}\right)\frac{1}{-i\omega + D_T k^2} + \frac{1}{2\gamma}\left(\frac{1}{-i\omega + \Gamma k^2 - ic_s k} + \frac{1}{-i\omega + \Gamma k^2 + ic_s k}\right) \tag{8.5.2}$$

which, via an inverse transform, yields an expression for $\rho_{\mathbf{k}}(t)$ given by

$$\rho_{\mathbf{k}}(t) = \rho_{\mathbf{k}}\left[\left(\frac{\gamma-1}{\gamma}\right)\exp\left(-D_T k^2 t\right) + \frac{1}{\gamma}\exp\left(-\Gamma k^2 t\right)\cos c_s k t\right] \quad (8.5.3)$$

The form of (8.5.3) shows that the purely imaginary root in (8.3.35) represents a fluctuation that decays without propagating, the lifetime of the fluctuation being determined by the thermal diffusivity defined by (8.3.36). By contrast, the complex roots correspond to a fluctuation that propagates through the fluid at the speed of sound, eventually decaying through the combined effects of viscosity and thermal conduction. The definition of Γ in (8.3.37) implies that the thermal damping of the sound mode is small when $\gamma \approx 1$, which is the case for many liquid metals. On multiplying through (8.5.3) by $\rho_{-\mathbf{k}}$, dividing by N and taking the thermal average, we obtain an expression for the density autocorrelation function $F(k,t)$; this is easily transformed to give

$$S(k,\omega) = \frac{S(k)}{2\pi}\left[\left(\frac{\gamma-1}{\gamma}\right)\frac{2D_T k^2}{\omega^2 + (D_T k^2)^2} + \frac{1}{\gamma}\left(\frac{\Gamma k^2}{(\omega + c_s k)^2 + (\Gamma k^2)^2} + \frac{\Gamma k^2}{(\omega - c_s k)^2 + (\Gamma k^2)^2}\right)\right] \quad (8.5.4)$$

The spectrum of density fluctuations therefore consists of three components: the *Rayleigh line*, centred at $\omega = 0$, and two *Brillouin lines* at $\omega = \pm c_s k$; a typical spectrum is plotted in Figure 8.4. The two shifted components correspond to propagating sound waves and are analogous to the longitudinal acoustic phonons of a solid, whereas the central line corresponds to the diffusive, thermal mode. The total integrated intensity of the Rayleigh line is

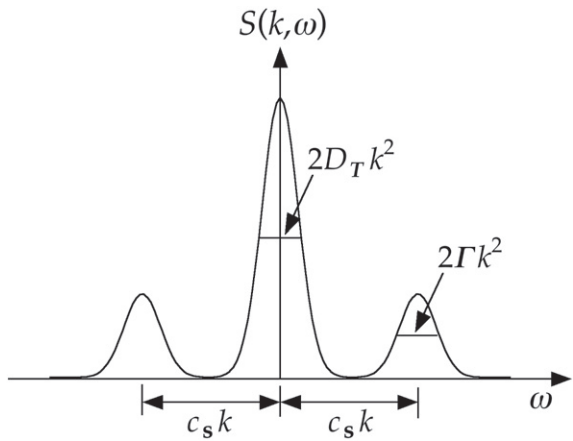

FIGURE 8.4 Dynamic structure factor in the hydrodynamic limit. D_T is the thermal diffusivity, Γ is the sound attenuation coefficient and c_s is the adiabatic speed of sound.

$$\mathcal{I}_{\mathrm{R}} = \frac{\gamma - 1}{\gamma} S(k) \tag{8.5.5}$$

and that of each of the two Brillouin lines is

$$\mathcal{I}_{\mathrm{B}} = \frac{1}{2\gamma} S(k) \tag{8.5.6}$$

Thus

$$\mathcal{I}_{\mathrm{R}} + 2\mathcal{I}_{\mathrm{B}} = S(k) \tag{8.5.7}$$

which is a particular case of the sum rule (7.4.23). The quantity

$$\frac{\mathcal{I}_{\mathrm{R}}}{2\mathcal{I}_{\mathrm{B}}} = \gamma - 1 \tag{8.5.8}$$

is called the Landau–Placzek ratio. As the values of c_P/c_V listed in Table 1.2 suggest, the Landau–Placzek ratio is typically an order of magnitude larger for the rare-gas liquids than for simple liquid metals. In passing from (8.5.1) to (8.5.2) we have, for sake of simplicity, omitted a non-Lorentzian term that in practice makes only a negligibly small, asymmetric correction to the Brillouin lines.[10]

We have chosen to discuss the behaviour of the longitudinal modes in terms of the local density and temperature, but it would have been equally appropriate to choose the pressure and entropy as variables, since these are also statistically independent (see Appendix A). The calculation is instructive because it shows that the first term in (8.5.2) can be identified with the decay of entropy fluctuations. It follows that the Brillouin doublet is associated with propagating pressure fluctuations at constant entropy (hence the appearance of the adiabatic speed of sound), while the Rayleigh line corresponds to non-propagating fluctuations in entropy at constant pressure.[4]

The wavelength of visible light is much greater than the nearest-neighbour spacing in liquids. Light scattering experiments are therefore ideally suited to measurements of the Rayleigh–Brillouin spectrum at long wavelengths and provide an accurate means of measurement of properties such as the thermal diffusivity, speed of sound and sound attenuation coefficient. However, the spectral lineshape is determined by a small number of macroscopic properties that are insensitive to details of either the interactions between particles or the molecular structure of the fluid. From the standpoint of microscopic theory the more interesting question is whether the propagating density fluctuations characteristic of the hydrodynamic regime can also be supported in simple liquids at wavelengths comparable with the spacing between particles. We have already seen in Section 7.5 that well-defined, collective excitations of the hydrodynamic type, manifesting themselves in a three-peak structure in $S(k, \omega)$, have been detected in neutron scattering experiments on liquid caesium, but comparable results have been obtained by neutron or X-ray scattering for the other alkali metals and for aluminium, gallium, magnesium

and mercury.[11] Brillouin-type side-peaks have also been seen in molecular dynamics simulations of a variety of systems, including both the hard-sphere[12] and Lennard-Jones[13] fluids. The spectra are therefore qualitatively similar to those predicted by hydrodynamics, though there are some major differences in detail. Figure 8.5, for example, shows the dispersion of the sound-wave peak observed in neutron scattering experiments on liquid caesium. At the smallest wavenumbers the dispersion is approximately linear, in agreement with hydrodynamics, but corresponds to a speed of propagation significantly higher than the experimental speed of sound. At larger wavenumbers the dispersion is no longer linear and eventually becomes negative. The widths of the Rayleigh and Brillouin lines are also poorly described by the hydrodynamic result. As we shall see in Section 8.6 and again in Chapter 9, a description of the density fluctuations in the range of k explored in neutron or X-ray scattering experiments requires a generalisation of the hydrodynamic approach, the effect of which is to replace the transport coefficients and thermodynamic derivatives in (8.5.4) by quantities dependent on frequency and wavenumber.

For later purposes we also require an expression for the hydrodynamic limit of the longitudinal current autocorrelation function $C_l(k,t)$. We proceed, as before, by solving the system of equations (8.3.26) for the variable of interest, which in this case is the longitudinal particle current $\tilde{j}^z_{\mathbf{k}}(z)$. The terms in $\rho_{\mathbf{k}}$ and

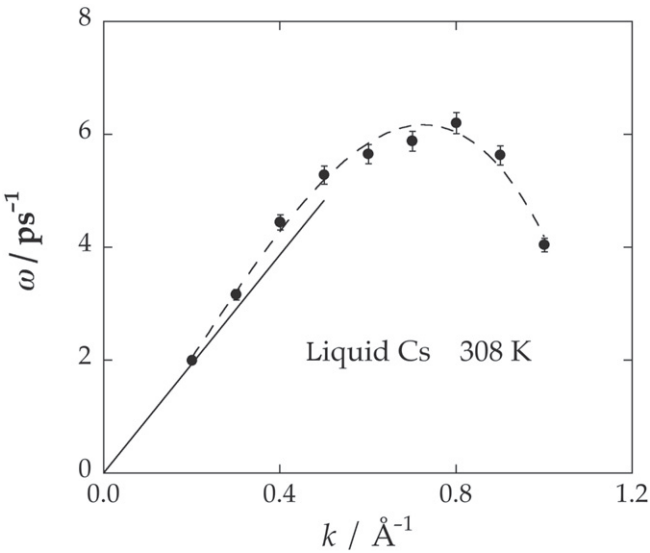

FIGURE 8.5 Dispersion of the Brillouin peak in liquid caesium near the normal melting temperature. The points are the results of inelastic neutron scattering experiments, the straight line shows the hydrodynamic dispersion corresponding to the experimental speed of sound, $c_S = 965$ m s^{-1}, and the dashed curve is a guide to the eye. After Bodensteiner et al.[14]

$T_{\mathbf{k}}$ may be omitted, since they are uncorrelated with $\tilde{j}^z_{-\mathbf{k}}$. For z on the real axis the result is

$$\tilde{j}^z_{\mathbf{k}}(\omega) = j^z_{\mathbf{k}} \frac{-i\omega(-i\omega + ak^2)}{D_l(k,\omega)} \tag{8.5.9}$$

Thus

$$\tilde{C}_l(k,\omega) = \frac{\omega_0^2}{-i\omega + bk^2 + c_s^2 k^2 \left(\frac{1}{-i\omega} + \frac{\gamma - 1}{-i\omega + ak^2}\right)} \tag{8.5.10}$$

Equation (8.5.10) shows that the spectrum of longitudinal current fluctuations at small k behaves as

$$C_l(k,\omega) = \frac{1}{\pi} \mathrm{Re}\, \tilde{C}_l(k,\omega) \approx \frac{\omega_0^2}{\pi\omega^2} \left(bk^2 + \frac{(\gamma - 1)ac_s^2 k^4}{\omega^2 + (ak^2)^2} \right) \tag{8.5.11}$$

Hence the longitudinal viscosity is given by a limiting operation analogous to (8.4.6) for the shear viscosity, i.e.

$$\frac{4}{3}\eta + \zeta = \rho m b = \lim_{\omega \to 0} \lim_{k \to 0} \frac{\omega^2}{k^4} C_l(k,\omega) \tag{8.5.12}$$

If we now follow steps similar to those that lead to the Green–Kubo formula (8.4.10), we find that the longitudinal viscosity can be expressed in terms of the autocorrelation function of a diagonal element of the microscopic stress tensor (8.4.14):

$$\frac{4}{3}\eta + \zeta = \lim_{\omega \to 0} \frac{\beta}{V} \int_0^\infty \left\langle \Pi_0^{zz}(t) \Pi_0^{zz} \right\rangle \exp(i\omega t) \mathrm{d}t \tag{8.5.13}$$

In taking the limit $\omega = 0$ in (8.5.13) we find a discontinuity: the thermal average of Π_0^{zz} is non-zero (see (8.4.15)), so the integrand in (8.5.13) approaches a non-zero value as $t \to \infty$. The problem is overcome by subtracting the invariant part, the transport coefficient being linked only to fluctuations in the local variables. Thus

$$\frac{4}{3}\eta + \zeta = \frac{\beta}{V} \int_0^\infty \left\langle \left[\Pi_0^{zz}(t) - PV\right]\left[\Pi_0^{zz} - PV\right] \right\rangle \mathrm{d}t \tag{8.5.14}$$

To obtain the Green–Kubo relation for the thermal conductivity we require an expression for the rate of decay of a fluctuation in $q(\mathbf{r},t)$, the macroscopic density of heat energy, which is related to the entropy density by (8.3.10). We first use (8.3.11) to eliminate the local temperature from the energy equation (8.3.13). The result is

$$\left(\frac{\partial}{\partial t} - a\nabla^2 \right) \delta q(\mathbf{r},t) - \frac{\lambda T \beta_V}{\rho^2 c_V} \nabla^2 \delta\rho(\mathbf{r},t) = 0 \tag{8.5.15}$$

which, after transformation to Fourier-Laplace variables and use of (8.3.12) together with the thermodynamic chain rule:

$$\left(\frac{\partial S}{\partial \rho}\right)_T = -\left(\frac{\partial S}{\partial T}\right)_\rho \left(\frac{\partial T}{\partial \rho}\right)_S = -\frac{Nc_V}{T}\left(\frac{\partial T}{\partial \rho}\right)_S \tag{8.5.16}$$

gives

$$\left(-iz + ak^2\right)\tilde{q}_{\mathbf{k}}(z) + \lambda k^2 \left(\frac{\partial T}{\partial \rho}\right)_S \tilde{\rho}_{\mathbf{k}}(z) = q_{\mathbf{k}} \tag{8.5.17}$$

Next, an equation relating $\tilde{\rho}_{\mathbf{k}}(z)$ to $\tilde{P}_{\mathbf{k}}(z)$ is obtained by taking the divergence of the Navier–Stokes equation (8.3.16) and transforming again to the variables k and z; the result in this case is

$$izm\left(-iz + bk^2\right)\tilde{\rho}_{\mathbf{k}}(z) - k^2\tilde{P}_{\mathbf{k}}(z) = -m\left(-iz + bk^2\right)\rho_{\mathbf{k}} \tag{8.5.18}$$

where $\mathbf{k}$ has once more been chosen perpendicular to the initial particle current. Equation (8.5.18) can now be converted into a relation for $\tilde{q}_{\mathbf{k}}(z)$ by making the substitutions

$$\tilde{P}_{\mathbf{k}}(z) = \left(\frac{\partial P}{\partial \rho}\right)_S \tilde{\rho}_{\mathbf{k}}(z) + \frac{V}{T}\left(\frac{\partial P}{\partial S}\right)_\rho \tilde{q}_{\mathbf{k}}(z) \tag{8.5.19}$$

and

$$\rho_{\mathbf{k}} = \left(\frac{\partial \rho}{\partial P}\right)_S P_{\mathbf{k}} + \frac{V}{T}\left(\frac{\partial \rho}{\partial S}\right)_\rho q_{\mathbf{k}} \tag{8.5.20}$$

The final step is to eliminate $\tilde{\rho}_{\mathbf{k}}(z)$ between (8.5.17) and (8.5.18). The resulting expression for $\tilde{q}_{\mathbf{k}}(z)$ has some similarities with that obtained previously for $\tilde{\rho}_{\mathbf{k}}(z)$ in (8.5.1). In particular, there are two complex conjugate poles and a single imaginary pole. At small k the local pressure and entropy are uncorrelated (see Appendix A). The problem can therefore be simplified by discarding terms proportional to $P_{\mathbf{k}}$. The lowest-order solution for $\tilde{q}_{\mathbf{k}}(z)$ then reduces to

$$\tilde{q}_{\mathbf{k}}(z) = \frac{q_{\mathbf{k}}}{-iz + D_T k^2} \tag{8.5.21}$$

Equation (8.5.21) describes a purely diffusive mode, thereby confirming the fact that the Rayleigh peak in $S(k, \omega)$ is associated with the decay of non-propagating entropy fluctuations.

Our main concern is with the behaviour at small k. Since $\lim_{k\to 0} q_{\mathbf{k}} = T\Delta S$, it follows from (A.8) of Appendix A that $\langle q_{\mathbf{k}} q_{-\mathbf{k}}\rangle$ can be replaced by

$$\left\langle q_0^2 \right\rangle = T^2 N k_{\mathrm{B}} c_P \tag{8.5.22}$$

We now proceed as in the cases of the shear and longitudinal viscosities. On multiplying (8.5.21) through by $q_{-\mathbf{k}}$ and taking the thermal average we obtain

an expression for the thermal conductivity of the form

$$\lambda = \rho c_P D_T = \frac{\beta}{VT} \lim_{\omega\to 0} \lim_{k\to 0} \frac{\omega^2}{k^2} \mathrm{Re}\, \langle \tilde{q}_{\mathbf{k}}(\omega) q_{-\mathbf{k}} \rangle \tag{8.5.23}$$

If we introduce a fluctuating heat current $\mathbf{J}^q_{\mathbf{k}}(t)$ defined, by virtue of (8.3.8), as the Fourier transform of

$$\mathbf{J}^q(\mathbf{r}, t) = \mathbf{J}^e(\mathbf{r}, t) - \frac{e + P}{\rho} \mathbf{j}(\mathbf{r}, t) \tag{8.5.24}$$

we see that the energy conservation equation (8.3.2) may be re-expressed as

$$\frac{\partial}{\partial t} q_{\mathbf{k}}(t) + i\mathbf{k} \cdot \mathbf{J}^q_{\mathbf{k}}(t) = 0 \tag{8.5.25}$$

Hence, if the z-axis is taken parallel to $\mathbf{k}$, we can rewrite (8.5.23) in typical Green-Kubo form as

$$\lambda = \frac{\beta}{VT} \int_0^\infty \left\langle J_0^{qz}(t) J_0^{qz} \right\rangle \mathrm{d}t \tag{8.5.26}$$

For (8.5.26) to be useful we require a microscopic expression for the heat current. On taking the Fourier transform of (8.3.2) we find that the component of the microscopic energy current in the direction of $\mathbf{k}$ is

$$-ikJ^{ez}_{\mathbf{k}} = \frac{\partial}{\partial t} e_{\mathbf{k}} = \frac{\partial}{\partial t} \sum_{i=1}^N \left(\frac{1}{2} m |\mathbf{u}_i|^2 + \frac{1}{2} \sum_{j\neq i}^N v(r_{ij}) \right) \exp(-i\mathbf{k} \cdot \mathbf{r}_i) \tag{8.5.27}$$

where we have adopted the convention that the interaction energy of a pair of particles is shared equally between them. Differentiation of the quantity inside large brackets gives rise to a term that can be treated by the methods used in calculating the microscopic stress tensor; the final result for $\mathbf{k} = 0$ is

$$J_0^{ez} = \sum_{i=1}^N u_{iz} \left(\frac{1}{2} m |\mathbf{u}_i|^2 + \frac{1}{2} \sum_{j\neq i}^N v(r_{ij}) \right) - \frac{1}{2} \sum_{i=1}^N \sum_{j\neq i}^N \mathbf{u}_i \cdot \mathbf{r}_{ij} \frac{\partial v(r_{ij})}{\partial z_{ij}} \tag{8.5.28}$$

The current J_0^{qz} is obtained from J_0^{ez} by subtracting the term $(e + P) \sum_i u_{iz}$; with a suitable choice of frame of reference this term will be zero. Thus we can equally well write the Green–Kubo formula for λ as

$$\lambda = \frac{\beta}{VT} \int_0^\infty \left\langle J_0^{ez}(t) J_0^{ez} \right\rangle \mathrm{d}t \tag{8.5.29}$$

The correlation function formulae (or the equivalent Einstein expressions) for D, η, ζ and λ have been used in simulations to determine the transport coefficients of a number of model systems. A particularly large body of results

exists for the hard-sphere fluid, some of which have already been discussed in Section 8.4. As we saw there, the shear viscosity is in good agreement with the predictions of Enskog theory at densities up to about 80% of that corresponding to the fluid-solid transition, but close to the transition it is larger than the Enskog value by a factor of nearly two. The enhancement of the shear viscosity at high densities is linked numerically to the existence of a long-lived, positive tail in the corresponding autocorrelation function. The bulk viscosity is purely potential in origin and vanishes as $\rho \to 0$, but the Enskog result for the thermal conductivity has a structure similar to that displayed for η in (8.4.21), i.e.

$$\frac{\lambda_E}{\lambda_0} = \frac{2\pi\rho d^3}{3}\left(\frac{1}{y} + 1.2 + 0.757y\right) \tag{8.5.30}$$

where y has the same meaning as before and $\lambda_0 = (75k_B/64d^2)(k_BT/\pi m)^{1/2}$ is the conductivity in the low-density limit.[5] The potential term (the last term within brackets) again provides the dominant contribution at high densities, but good agreement with molecular dynamics results is now maintained up to the freezing transition, as Figure 8.6 reveals. The greater success of Enskog theory in the case of the thermal conductivity can plausibly be linked to the fact that there is no significant tail in the energy current autocorrelation function, which is a featureless curve that decays smoothly to zero.

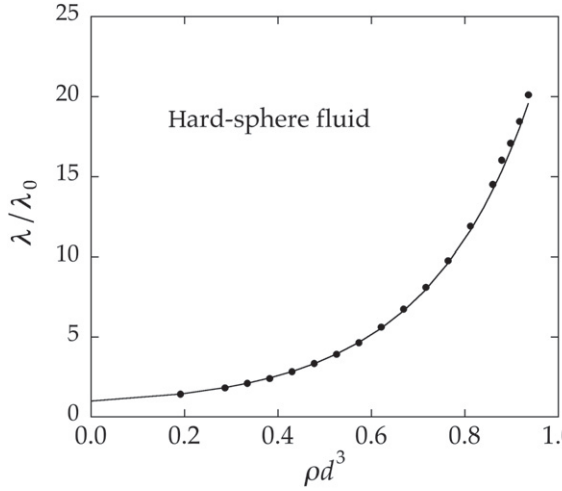

FIGURE 8.6 Thermal conductivity of the hard-sphere fluid as a function of density relative to its value in the low-density limit. The points are the results of molecular dynamics calculations[15] and the curve is the Enskog approximation (8.5.30).

8.6 GENERALISED HYDRODYNAMICS

In the earlier sections of this chapter we have shown in some detail how the equations of hydrodynamics can be used to calculate the time correlation functions of conserved variables in the long-wavelength, low-frequency limit. Two questions then arise. First, what are the scales of length and time over which it is possible to maintain the continuum description that underlies the hydrodynamic approach? Secondly, how may the hydrodynamic equations be modified to make their predictions applicable on the atomic scale, where lengths are typically of order a few ångström units and times are of order 10^{-13} s? We have seen in Chapter 7 that the behaviour of the correlation functions at short times is related to frequency sum rules involving static distribution functions descriptive of the molecular structure of the fluid. It is precisely these sum rules that are violated by hydrodynamic expressions such as (8.4.5) and (8.5.4), since the resulting frequency moments beyond zeroth order all diverge. In addition, an exponential decay, such as that in (8.4.3), cannot satisfy certain of the general properties of time correlation functions discussed in Section 7.1. The failure of the hydrodynamic approach at short times (or high frequencies) is linked to the presence of dissipative terms in the basic hydrodynamic equations; the latter, unlike the microscopic equations of motion, are not invariant under time reversal. In this section we describe some phenomenological generalisations of the hydrodynamic equations, based on the introduction of frequency and wavenumber-dependent transport coefficients, that have been developed in attempts to bridge the gap between the hydrodynamic (small k, ω) and kinetic (large k, ω) regimes. The use of non-local transport coefficients is closely related to the memory function approach of Section 7.3, which we develop in more systematic fashion in Chapter 9.

The ideas of *generalised hydrodynamics* are most easily illustrated by considering the example of the transverse current correlations. Equation (8.4.3) shows that in the hydrodynamic limit the correlation function $C_t(k,t)$ decays exponentially with a relaxation time equal to $1/\nu k^2$, where ν is the kinematic shear viscosity. The corresponding power spectrum is of Lorentzian form:

$$C_t(k,\omega) = \frac{1}{\pi}\mathrm{Re}\,\tilde{C}_t(k,\omega) = \frac{\omega_0^2}{\pi}\frac{\nu k^2}{\omega^2 + (\nu k^2)^2} \tag{8.6.1}$$

The ω^{-2} behaviour at large ω is not compatible with the exact, high-frequency sum rules such as (7.4.38), nor does (8.6.1) yield the correct free-particle limit of $C_t(k,\omega)$ at large k; that limit is gaussian in form, similar to the longitudinal free-particle limit displayed in (7.5.17). Moreover, molecular dynamics calculations, which are the only source of 'experimental' information on transverse current fluctuations in atomic liquids, show that in an intermediate wavenumber range $C_t(k,t)$ decays in an oscillatory manner and its power spectrum has a peak at non-zero frequency, suggestive of the existence of a propagating shear mode. (Examples of the power spectra are shown later in Chapter 9, Figure 9.4.)

What this implies physically is that at high frequencies the fluid has insufficient time to flow in response to an applied strain rate, and instead reacts elastically in the manner of a solid. To account for the appearance of shear waves we need to extend the hydrodynamic description to include the effects of elasticity. Suppose that a shearing force is applied to a fluid. The strain at a point (x, y, z) is expressible in terms of the displacement $\mathbf{r}$ at that point and the rate of strain is expressible in terms of the velocity $\dot{\mathbf{r}}$. If the flow is purely viscous, the shearing stress (an off-diagonal component of the stress tensor $\mathbf{\Pi}$) is proportional to the rate-of-strain tensor and may be written as

$$\Pi^{xz} = -\eta \frac{\partial}{\partial t}\left(\frac{\partial r_x}{\partial z} + \frac{\partial r_z}{\partial x}\right) \tag{8.6.2}$$

which is the hydrodynamic form (see (8.3.15)). By contrast, if the force is applied suddenly, the instantaneous displacement is determined by the stress through a typical stress-strain relation, i.e.

$$\Pi^{xz} = -G_\infty \left(\frac{\partial r_x}{\partial z} + \frac{\partial r_z}{\partial x}\right) \tag{8.6.3}$$

where G_∞ is an instantaneous (high-frequency) modulus of rigidity. We can interpolate between these two extremes by making a *viscoelastic* approximation such that

$$\left(\frac{1}{\eta} + \frac{1}{G_\infty}\frac{\partial}{\partial t}\right)\Pi^{xz} = -\frac{\partial}{\partial t}\left(\frac{\partial r_x}{\partial z} + \frac{\partial r_z}{\partial x}\right) \tag{8.6.4}$$

By taking the Laplace transform of (8.6.4) it is easy to show that the viscoelastic approximation is equivalent to replacing η in (8.6.2) by a complex, frequency-dependent, shear viscosity given by

$$\tilde{\eta}(\omega) = \frac{G_\infty}{-i\omega + \tau_{\mathrm{M}}^{-1}} \tag{8.6.5}$$

The constant $\tau_M = \eta/G_\infty$ is called the Maxwell relaxation time. If $\omega\tau_M \ll 1$, $\tilde{\eta}(\omega) \approx \eta$, which corresponds to purely viscous flow, but if $\omega\tau_M \gg 1$, substitution of (8.6.5) in (8.6.4) yields a dispersion relation of the form $\omega^2 \approx \left(G_\infty/\rho m\right) k^2$, corresponding to elastic waves propagating at a speed

$$c_t = \left(G_\infty/\rho m\right)^{1/2} \tag{8.6.6}$$

Figure 8.7 shows the dispersion of the shear-wave peak observed in molecular dynamics simulations of liquid argon and liquid potassium at state conditions close to their respective triple points. Over the wavenumber range covered by the figure the dispersion is well described by a relation of the form $\omega = c_t(k - k_t)$, where k_t is the wavenumber below which the propagating mode vanishes. In the case of argon, for which a value of G_∞ is available from

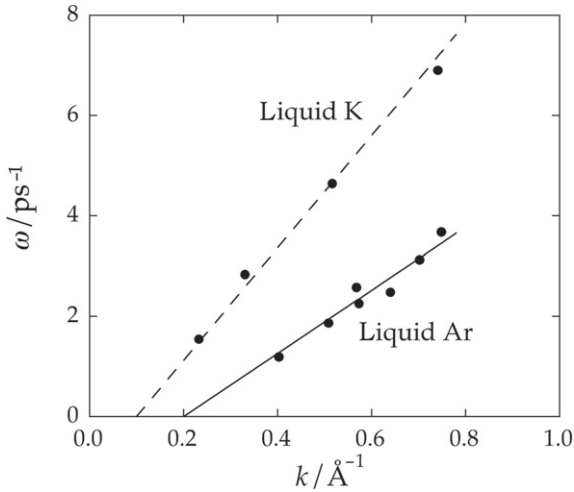

FIGURE 8.7 Dispersion of the shear-wave peak derived from molecular dynamics simulations of liquid argon[13,16] and liquid potassium[17] for state conditions close to the triple point. The dashed line through the data for potassium is a guide to the eye; the full line for argon is drawn with a slope given by the viscoelastic expression (8.6.6) for the speed of propagation (630 m s^{-1}). Results are shown only for the range of k in which the dispersion is approximately linear.

simulation, the slope of the dispersion curve is in surprisingly good agreement with that calculated from the viscoelastic approximation (8.6.6).

If account is to be taken of non-local effects in space the generalised shear viscosity must be a function of wavenumber as well as of frequency. The rigidity modulus is also dependent on k and related in a simple way to the second frequency moment ω_{1t}^2. These ideas can be formalised via a phenomenological generalisation of the hydrodynamic equation (8.4.2):

$$\frac{\partial}{\partial t}C_t(k,t) + k^2 \int_0^\infty \nu(k, t-s)C_t(k,s)\mathrm{d}s = 0 \tag{8.6.7}$$

The quantity $\nu(k,t)$ is a memory function; it describes a response that is non-local in both space and time and its Laplace transform $\tilde{\nu}(k,\omega)$ plays the role of a generalised kinematic shear viscosity. If we take the Laplace transform of (8.6.7) and compare the result with (8.4.4), we find that $\tilde{\nu}(k,\omega)$ must satisfy the constraint that

$$\lim_{\omega\to 0}\lim_{k\to 0}\tilde{\nu}(k,\omega) = \nu \tag{8.6.8}$$

where ν is the macroscopic transport coefficient, given (apart from a factor ρm) by the Green–Kubo formula (8.4.10). If, on the other hand, we differentiate (8.6.7) with respect to t, set $t = 0$ and use (7.4.37), we find that

$$\nu(k, t=0) = \frac{\omega_{1t}^2}{k^2} \equiv \frac{G_\infty(k)}{\rho m} \tag{8.6.9}$$

which acts as the definition of the k-dependent shear modulus $G_\infty(k)$. Equations (8.6.8) and (8.6.9) are useful in the construction of approximate forms of $\nu(k,t)$ that reduce to the hydrodynamic and viscoelastic expressions in the limits, respectively, $\omega \to 0$ and $\omega \to \infty$.

If molecular dynamics results for $C_t(k,t)$ are available, values of the generalised shear viscosity $\tilde{\eta}(k,\omega) = \rho m \tilde{\nu}(k,\omega)$ can be obtained by numerical inversion of (8.6.7) while its value at infinite wavelength, $\tilde{\eta}(k=0,\omega) \equiv \tilde{\eta}(\omega)$, is given by the Laplace transform of the stress autocorrelation function $\eta(t)$ in (8.4.10). The generalised shear viscosity is believed to be a non-analytic function of both k and ω. For example, molecular dynamics calculations for hard spheres[18] have shown that $\eta(t)$ decays as $t^{-3/2}$ beyond about ten mean collision times, implying that $\tilde{\eta}(\omega)$ behaves as $\omega^{1/2}$ at low frequencies. If the zero-frequency shear viscosity $\eta(k) \equiv \tilde{\eta}(k,\omega=0)$ could be expanded in a Taylor series in k about its macroscopic limit, $\eta \equiv \eta(0)$, the series would start as

$$\eta(k) = \eta + \eta_2 k^2 + \cdots \tag{8.6.10}$$

since invariance under space inversion means that only even powers of k can appear. The quantity η_2 is called a Burnett coefficient. Burnett coefficients were introduced in an attempt to extend the range of validity of hydrodynamic equations through the addition of terms of higher order in the gradients of the hydrodynamic fields. However, the indications from mode coupling theories[19] of the type to be discussed in the section that follows are that the coefficients diverge, implying that the relation between the applied gradients and the induced hydrodynamic fluxes is non-analytic in character. This conclusion is supported by the results of computer simulations of a soft-sphere (r^{-12}) fluid[20], which are compatible with a small-k behaviour of the form

$$\eta(k) = \eta - \eta_{3/2} k^{3/2} + \cdots \tag{8.6.11}$$

where $\eta_{3/2}$ is a positive quantity. These and related calculations[21] suggest that $\eta(k)$ and other generalised transport coefficients decrease smoothly with increasing wavenumber, becoming an order of magnitude smaller than their macroscopic ($k=0$) values when the wavelength is comparable with the inter-particle spacing.

The longitudinal projections of the hydrodynamic equations may be treated in the same way through the introduction of wavenumber and frequency-dependent quantites that are generalisations of the coefficients a and b defined by (8.3.14) and (8.3.25). Similarly, the thermodynamic derivatives, which are related to static correlation functions, become functions of wavelength.[22] In particular, the macroscopic compressibility is replaced by its k-dependent generalisation, i.e. the structure factor $S(k)$ (see (3.6.11)), while the thermal pressure coefficient, which determines the coupling between momentum and energy, now contains a part that is explicitly dependent on frequency and vanishes in the limit $k \to 0$. A scheme in which the various thermodynamic

and transport coefficients are assumed to be functions only of wavenumber and not of frequency has been found to reproduce satisfactorily a large part of the molecular dynamics results obtained for the dynamic structure factor of the hard-sphere fluid.[12] This approach breaks down, however, both for wavelengths shorter than the mean free path, corresponding to free-particle behaviour, and at densities close to crystallisation, where viscoelastic effects becomes important.

8.7 LONG-TIME TAILS IN TIME CORRELATION FUNCTIONS

Fluctuations in the conserved hydrodynamic variables decay infinitely slowly in the long-wavelength limit. The rates of relaxation are determined by the hydrodynamic eigenvalues (8.3.31) and (8.3.35) (multiplied by $-i$), all of which vanish with k. No such property holds for the non-conserved currents that enter the Green–Kubo integrands for the transport coefficients; if it did, the transport coefficients would not be well defined. Until the late 1960s it was generally believed that away from critical points the autocorrelation functions of non-conserved variables decay exponentially at long times. This, for example, is the behaviour predicted by the Boltzmann and Enskog equations. It therefore came as a surprise when analysis of the molecular dynamics results of Alder and Wainwright[23] on self diffusion in hard-disk ($\mathcal{D} = 2$) and hard-sphere ($\mathcal{D} = 3$) fluids showed that the velocity autocorrelation function apparently decays asymptotically as $t^{-\mathcal{D}/2}$, where $\mathcal{D}$ denotes the dimensionality of the system. Later simulations of hard-core fluids and other systems have also detected the presence of a long-time tail in the stress tensor autocorrelation function.

The presence of a slowly decaying tail in $Z(t)$ suggests that highly collective effects make a significant contribution to the process of self diffusion. The apparent involvement of large numbers of particles makes it natural to analyse the long-time behaviour in hydrodynamic terms, and Alder and Wainwright were led in this way to a simple but convincing explanation of their results. Underlying their argument is the idea that the initial motion of a tagged particle creates around that particle a vortex, which in turn causes a retarded current to develop in the direction of the initial velocity. At low densities, where the initial direction of motion is likely to persist, the effect of the current is to reduce the drag on the particle, thereby propelling it onwards in the forward direction. This results in a long-lasting, positive correlation between the initial velocity and its value at later times. At high densities, on the other hand, the initial direction of motion is on average soon reversed. In this case the retarded current gives rise to an extra drag at later times, causing $Z(t)$ to change sign; at very large times an enhancement of the forward motion can again be expected, but the effect is likely to be undetectable. That this physical picture is basically correct

was confirmed in striking fashion by observation of the velocity field that forms around a moving particle in a fluid of hard disks. A vortex pattern quickly develops, which after a few mean collision times matches closely the pattern obtained by numerical solution of the Navier–Stokes equation. The persistence of the tail in $Z(t)$ is therefore associated with a coupling between the motion of the tagged particle and the hydrodynamic modes of the fluid. As we shall now show, this argument can be formalised in such a way as to predict the observed $t^{-\mathcal{D}/2}$ decay at long times.[24]

Suppose that at time $t = 0$ a particle i has a component of velocity $u_{ix}(0)$ in the x-direction. After a short time, τ say, collisions will have caused the initial momentum of particle i to be shared among the ρV_τ particles in a $\mathcal{D}$-dimensional volume V_τ centred on i. Local equilibrium now exists within the volume V_τ, and particle i will be moving with a velocity $u_{ix}(\tau) \approx u_{ix}(0)/\rho V_\tau$. (We have assumed, for simplicity, that the neighbours of i are initially at rest.) Further decay in the velocity $u_{ix}(t)$ for $t > \tau$ will occur as the result of enlargement of the volume V_τ, i.e. from the spread of the velocity field around particle i. At large times the dominant contribution to the growth of V_τ will come from diffusion of the transverse component of the velocity field and the radius of V_τ will therefore increase as $(\nu t)^{1/2}$. Thus $V_\tau \sim (\nu t)^{3/2}$ in the three-dimensional case, from which it follows that $Z(t) \sim (\nu t)^{-3/2}$. This argument assumes that particle i remains at the centre of V_τ; if the diffusive motion of i is taken into account it can be shown that

$$Z(t) \sim \left[(D + \nu)t\right]^{-3/2} \tag{8.7.1}$$

The analogous result in two dimensions implies that a self-diffusion coefficient does not exist, because the integral of $Z(t)$ diverges logarithmically.

The form of (8.7.1) has been confirmed by a number of more sophisticated calculations. In the case of hard-core fluids these include a microscopic treatment based on kinetic theory in which account is taken of the effect of correlated collision sequences (the ring collisions of Section 7.2) along with that of uncorrelated, binary collisions.[25] Though limited to low densities, the calculation shows that the velocity, stress tensor and energy current autocorrelation functions all decay as $t^{-\mathcal{D}/2}$; it also yields explicit expressions for the coefficients of the long-time tails. A more phenomenological approach has also been developed in which the existence of the long-time tails is explained by simple arguments concerning the decay of fluctuations into pairs of hydrodynamic modes. Since the physical content of this work is closely related to the mode coupling formalism to be discussed in Chapter 9, we give here a brief derivation of the result obtained in three dimensions for the velocity autocorrelation function.[26]

The definition (7.1.3) of a time correlation function involves an equilibrium ensemble average over the initial phase space coordinates of the system. This average can be replaced by a constrained ensemble average, characterised by an initial position $\mathbf{r}_0$ and initial velocity $\mathbf{u}_0$ of a tagged particle i, which is then

integrated over all $\mathbf{r}_0$ and $\mathbf{u}_0$. The definition of $Z(t)$ is thereby reformulated as

$$Z(t) = \langle u_{ix}(t)u_{ix}\rangle = \int \mathrm{d}\mathbf{r}_0 \int \mathrm{d}\mathbf{u}_0\, u_{0x}\, \langle u_{ix}(t)\delta(\mathbf{u}_i - \mathbf{u}_0)\delta(\mathbf{r}_i - \mathbf{r}_0)\rangle \tag{8.7.2}$$

The constrained average in (8.7.2) can be written as a non-equilibrium ensemble average (subscript n.e.) defined through the relation

$$\langle u_{ix}(t)\delta(\mathbf{u}_i - \mathbf{u}_0)\delta(\mathbf{r}_i - \mathbf{r}_0)\rangle = \langle u_{ix}(t)\rangle_{\text{n.e.}}\, \langle \delta(\mathbf{u}_i - \mathbf{u}_0)\delta(\mathbf{r}_i - \mathbf{r}_0)\rangle \tag{8.7.3}$$

In the canonical ensemble the equilibrium average on the right-hand side of (8.7.3) is equal to $1/N$ times the single-particle distribution function defined by (2.1.15) (taken for $n = 1$) but with $\mathbf{p}$ replaced by $\mathbf{u}$ as independent variable. Equations (8.7.2) and (8.7.3) may therefore be combined to give

$$Z(t) = \frac{1}{V}\int \mathrm{d}\mathbf{r}_0 \int \mathrm{d}\mathbf{u}_0\, \phi_{\text{M}}(\mathbf{u}_0)u_{0x}\, \langle u_{ix}(t)\rangle_{\text{n.e.}} \tag{8.7.4}$$

where $\phi_{\text{M}}(\mathbf{u}_0)$ is the Maxwell distribution (2.1.28). By defining a tagged-particle distribution function in the non-equilibrium ensemble as

$$f^{(s)}(\mathbf{r}, \mathbf{u}; t) = \big\langle \delta\left[\mathbf{r}_i(t) - \mathbf{r}\right]\delta[\mathbf{u}_i(t) - \mathbf{u}]\big\rangle_{\text{n.e.}} \tag{8.7.5}$$

we can rewrite the non-equilibrium average in (8.7.4) as

$$\langle u_{ix}(t)\rangle_{\text{n.e.}} = \int \mathrm{d}\mathbf{r} \int \mathrm{d}\mathbf{u}\, u_x f^{(s)}(\mathbf{r}, \mathbf{u}; t) \tag{8.7.6}$$

The calculation thus far is exact. To make progress we assume that $f^{(s)}(\mathbf{r}, \mathbf{u}; t)$ relaxes towards the corresponding local equilibrium form on a time scale that is fast in comparison with the rate of decay of $Z(t)$. The long-time behaviour of the non-equilibrium average (8.7.6) is then obtained by replacing $f^{(s)}(\mathbf{r}, \mathbf{u}; t)$ by the tagged-particle analogue of (8.1.5) to give

$$\langle u_{ix}(t)\rangle_{\text{n.e.}} = \int \rho^{(s)}(\mathbf{r}, t)u_x(\mathbf{r}, t)\mathrm{d}\mathbf{r} \tag{8.7.7}$$

If this result is in turn substituted in (8.7.4), and the hydrodynamic variables $\mathbf{u}(\mathbf{r}, t)$ and $\rho^{(s)}(\mathbf{r}, t)$ are replaced by the sums of their Fourier components, we find that

$$\begin{aligned} Z(t) = \frac{1}{3V}\int \mathrm{d}\mathbf{r}_0 \int \mathrm{d}\mathbf{u}_0\, \phi_{\text{M}}(\mathbf{u}_0)\frac{1}{V^2}\sum_{\mathbf{k}}\sum_{\mathbf{k}'}\rho^{(s)}_{\mathbf{k}'}(t) \\ \times\, \mathbf{u}_{\mathbf{k}}(t)\cdot\mathbf{u}_0 \int \exp[-i(\mathbf{k}+\mathbf{k}')\cdot\mathbf{r}]\mathrm{d}\mathbf{r} \end{aligned} \tag{8.7.8}$$

The integral over $\mathbf{r}$ is equal to $V\delta_{\mathbf{k},-\mathbf{k}'}$ and (8.7.8) therefore reduces to

$$Z(t) = \frac{1}{3V}\int \mathrm{d}\mathbf{r}_0 \int \mathrm{d}\mathbf{u}_0\, \phi_{\text{M}}(\mathbf{u}_0)\frac{1}{V}\sum_{\mathbf{k}}\rho^{(s)}_{-\mathbf{k}}(t)\mathbf{u}_{\mathbf{k}}(t)\cdot\mathbf{u}_0 \tag{8.7.9}$$

Equation (8.7.9) is said to be of 'mode coupling' form because $Z(t)$ is expressed as a sum of products of pairs of hydrodynamic variables. We assume, in addition, that at times much longer than the mean collision time the decay of $Z(t)$ is dominated by the long-wavelength components of the hydrodynamic fields and that the time evolution of the latter is described by the equations of linearised hydrodynamics. The quantity $\rho_{-\mathbf{k}}^{(s)}(t)$ is then given by (8.2.5), while the hydrodynamic velocity field is conveniently divided into its longitudinal and transverse parts:

$$\mathbf{u}_{\mathbf{k}}(t) = \mathbf{u}_{\mathbf{k}l}(t) + \mathbf{u}_{\mathbf{k}t}(t) \tag{8.7.10}$$

The term $\mathbf{u}_{\mathbf{k}t}(t)$ satisfies the transverse current diffusion equation (8.4.1) (with $\mathbf{j}_{\mathbf{k}t} = \rho\mathbf{u}_{\mathbf{k}t}$), the solution to which is

$$\mathbf{u}_{\mathbf{k}t}(t) = \mathbf{u}_{\mathbf{k}t} \exp(-\nu k^2 t) \tag{8.7.11}$$

The longitudinal velocity field may be treated in a similar way, but its contribution to $Z(t)$ turns out to decay exponentially, the physical reason for this being the fact that the momentum of the tagged particle is carried away by the propagating sound waves. Hence the long-time behaviour of $Z(t)$ is entirely determined by the transverse velocity field. Finally, the choice of initial conditions implies that

$$\rho_{-\mathbf{k}}^{(s)} = \exp(i\mathbf{k}\cdot\mathbf{r}_0) \tag{8.7.12}$$

and

$$\mathbf{j}_{\mathbf{k}} = \rho\mathbf{u}_{\mathbf{k}} = \mathbf{u}_0 \exp(-i\mathbf{k}\cdot\mathbf{r}_0) \tag{8.7.13}$$

An expression for $Z(t)$ is now obtained by substituting (8.7.11), (8.7.12) and the transverse projection of (8.7.13) into (8.7.9) (remembering that there are two transverse components), and integrating over $\mathbf{r}_0$ and $\mathbf{u}_0$. The result is

$$Z(t) = \frac{2k_{\mathrm{B}}T}{3\rho m V}\sum_{\mathbf{k}} \exp\left[-(D+\nu)k^2 t\right] \tag{8.7.14}$$

or, in the thermodynamic limit:

$$Z(t) = \frac{2k_{\mathrm{B}}T}{3\rho m}(2\pi)^{-3}\int \exp\left[-(D+\nu)k^2 t\right]\mathrm{d}\mathbf{k} \tag{8.7.15}$$

Integration over all wavevectors is a questionable procedure, since the hydrodynamic equations on which (8.7.15) is based are not valid when k is large. However, we are interested only in the asymptotic form of $Z(t)$, and the main contribution to the integral comes from wavenumbers such that $k \approx [(D+\nu)t]^{-1/2}$; this is in the hydrodynamic range whenever t is much larger than typical microscopic times ($\sim 10^{-13}$) s. Alternatively, a natural upper limit on k can be introduced by a more careful choice of the initial spatial distribution

of tagged particles. Use of such a cut-off has no effect on the predicted long-time behaviour that results from carrying out the integration in (8.7.15), namely

$$Z(t) \sim \frac{2k_B T}{3\rho m}\left[4\pi(D+\nu)t\right]^{-3/2}, \quad t \to \infty \tag{8.7.16}$$

This result has the same general form as (8.7.1) but it also provides an explicit expression for the coefficient of the long-time tail.

The result in (8.7.16) has been confirmed by molecular dynamics calculations for systems of hard discs and of particles interacting through a Lennard-Jones potential truncated at $r = 2^{1/6}\sigma$, the separation at which $v(r)$ has its minimum value; the simulations are difficult to carry out with the necessary precision because the long-time tail is very weak.[28] Results obtained for the truncated Lennard-Jones potential are shown in Figure 8.8, where $Z(t)$ is plotted versus t on a log-log scale. If (5.4.5) is used to define an effective hard-sphere diameter for the particles, the onset of the asymptotic behaviour is found to come after approximately 18 mean collision times. The predicted long-time behaviour of $Z(t)$ implies that at low frequencies its Fourier transform behaves as

$$Z(\omega) = \frac{D}{\pi}\left[1 - (\omega_0/\omega)^{1/2} + \cdots\right] \tag{8.7.17}$$

where ω_0 is related to the transport coefficients D and ν. Experimentally, evidence for the presence of a long-time tail can be derived from neutron scattering measurements of the self dynamic structure factor, provided results are obtained at sufficiently small values of k to allow the extrapolation required

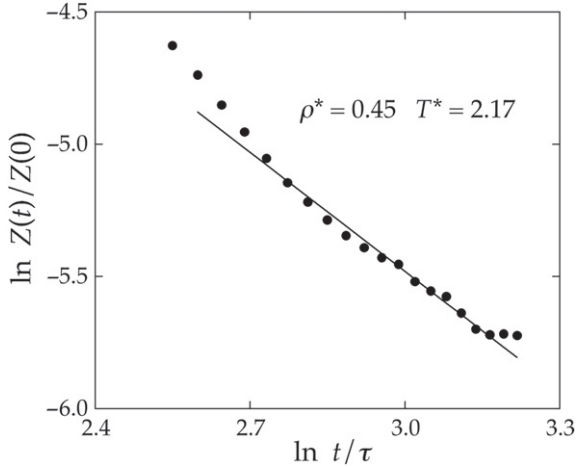

FIGURE 8.8 Log-log plot of the velocity autocorrelation function versus time for a system of particles interacting through a truncated Lennard-Jones potential. The points are molecular dynamics results and the line is drawn with a slope equal to $-3/2$. The unit of time is $\tau = (m\sigma^2/48\epsilon)^{1/2}$. *Redrawn with permission from Ref. 27 © 1974 American Physical Society.*

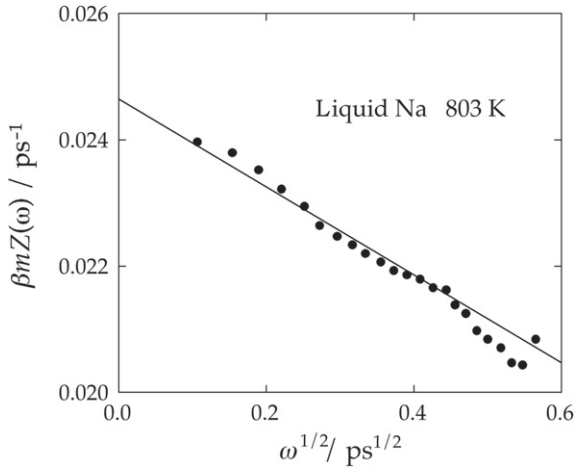

FIGURE 8.9 Power spectrum of the velocity autocorrelation function of liquid sodium as a function of $\omega^{1/2}$. The points are derived from inelastic neutron scattering measurements and the line is a least-squares fit to the data. *Redrawn with permission from Ref. 29 © 1987 American Physical Society.*

in (8.2.18) to be successfully carried through. Figure 8.9 shows some results obtained for liquid sodium at a temperature well above the melting point; at low temperatures the effect is too weak to be detectable. Not only is the square-root dependence on ω well reproduced, but the value obtained for ω_0 from a least-squares fit to the data lies within 2% of that predicted by mode coupling theory.

8.8 DYNAMICS OF SUPERCOOLED LIQUIDS

We know from Section 6.10 that when a liquid is quenched rapidly to temperatures below the freezing temperature T_f it may, rather than crystallising, undergo a transition to a glassy state at a glass transition temperature T_G. The freezing out of the translational and rotational degrees of freedom at the glass transition leads in many cases to anomalies in the temperature dependence of thermodynamic properties such as the specific heat. The change in behaviour at T_G is therefore described as a 'thermodynamic' or 'calorimetric' phase transition, though its nature is very different from that of an equilibrium phase transition. Section 6.10 was concerned with thermodynamic properties and the possible existence of an underlying ideal glass state; in this section we discuss the microscopic dynamics of liquids in the temperature range between T_f and T_G.

Relaxation times in the supercooled liquid measured, for example, in dielectric or shear stress relaxation experiments, increase dramatically with decreasing temperature; close to the glass transition they become comparable with macroscopic time scales. A rough but useful estimate of T_G is provided by the viscoelastic theory of Section 8.6, which shows that a crossover from viscous to elastic behaviour can be expected when the structural relaxation time of the system becomes comparable with the Maxwell relaxation time, defined as the ratio of shear viscosity to shear modulus, $\tau_M = \eta/G_\infty$. The shear modulus is of order 10^9 N m^{-2} for most materials and is only weakly dependent on temperature, but the shear viscosity rises by many orders of magnitude as the temperature approaches T_G. An implicit definition of T_G is obtained by identifying τ_M with some experimental time scale, τ_{exp}. A choice of 10^3 s for τ_{exp} leads to the conventional definition of T_G as the temperature at which the viscosity reaches a value of 10^{13} poise (1 P $\equiv$ 0.1 N m^{-2} s).

Glass forming liquids fall into one of two broad classes: 'strong' and 'fragile'.[30] The difference between the two is particularly evident in the way in which the viscosity changes with temperature, as exemplified by the Arrhenius plots shown in Figure 8.10. Strong glass formers are covalently bonded, network forming substances such as silica; the network already exists in the high-temperature melt and gradually strengthens as the liquid is supercooled. The calorimetric anomalies near T_G are weak, or may be absent altogether, and the Arrhenius plots are essentially linear, implying that transport in the liquid is

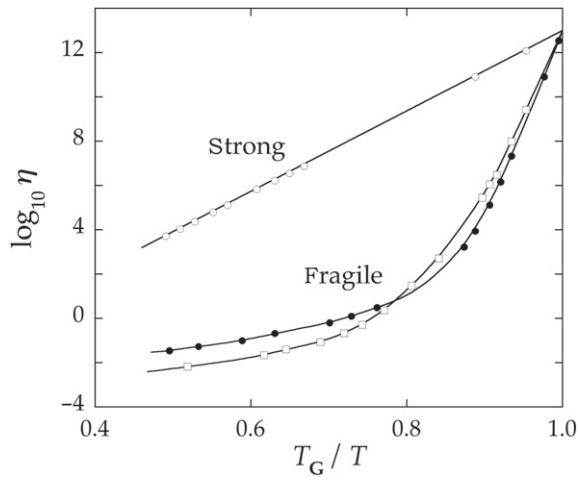

FIGURE 8.10 Arrhenius plots of the shear viscosities (in poise) of three glass-forming liquids, showing the difference in behaviour between strong and fragile glass formers. Open circles: silica; squares: o-terphenyl; filled circles: an ionic melt of composition $[KNO_3]_{0.6}[Ca(NO_3)_2]_{0.4}$. From C.A. Angell, 'Perspective on the glass transition', *J. Phys. Chem. Solids* **49**, 863–871 (1988), *with permission of Elsevier.*

largely governed by thermally activated processes or 'barrier hopping'. The anomalies are greater for the ionic and organic liquids that make up the class of fragile glass formers. Arrhenius plots for such materials show a marked change in curvature at a temperature T_C lying some 10–20% above T_G; this is suggestive of a qualitative change in character of the microscopic dynamics over a narrow temperature interval. When $T \approx T_C$, the Maxwell relaxation time is in the nanosecond range. This is a time scale well suited to studies of the dynamics by neutron and light scattering experiments and other experimental probes as well as by molecular dynamics simulation, and there is now ample evidence to show that as the temperature is lowered towards T_C there is a dramatic slowing down in the decay of time-dependent correlation functions. The crossover in behaviour near T_C seen, for example, in Figure 8.10, corresponds to what is called a *kinetic glass transition*. Experiment and simulation also show that structural and thermodynamic properties vary smoothly with temperature in the region of the transition. It is therefore reasonable to suppose that the supercooled liquid remains in a state of thermodynamic equilibrium and that equilibrium statistical mechanics applies once crystallisation has been by-passed. This is the key assumption underlying the mode coupling theory of the transition, described later in Section 9.6.

The nature of the changes that take place at the kinetic glass transition are well illustrated by the results shown in Figures 8.11 and 8.12. Those in Figure 8.11 are taken from a simulation of a binary,[31] soft-sphere (r^{-12}) fluid[32] and show the behaviour for one of the two species of the probability density

$$W(r,t) = 4\pi r^2 G_s(r,t) \tag{8.8.1}$$

where $G_s(r,t)$ is the self part of the van Hove function (7.4.19); the quantity $W(r,t)\mathrm{d}r$ is the probability of finding a particle at time t at a distance in the range r to $r + \mathrm{d}r$ from its position at $t = 0$. The thermodynamic state of the system is specified by a single coupling constant, Γ, defined in a manner similar to (5.4.13) but generalised to allow for the two-component nature of the system. A decrease in temperature is therefore strictly equivalent to an increase in density. The inset to the figure shows the results obtained for three different times at a value of Γ corresponding to a temperature above T_C. The curve has a single peak, which moves to larger r according to a $t^{1/2}$ law, in agreement with the result derived from Fick's law (see (8.2.8)). However, the qualitative behaviour changes dramatically above a threshold value of Γ, which can be identified with the crossover value Γ_C. The peak in $W(r,t)$ now appears frozen at a fixed value of r and its amplitude decreases only slowly with time as a secondary maximum builds up at a distance from the main peak roughly equal to the mean spacing between particles. The physical interpretation of this bimodal distribution is clear: most atoms vibrate around fixed, disordered positions, but some diffuse slowly by correlated hopping to neighbouring sites. The two values of Γ for which the results are shown correspond to temperatures differing by less

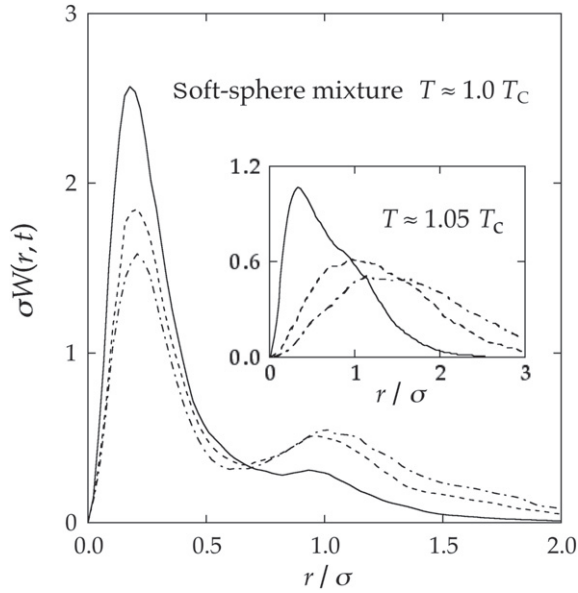

FIGURE 8.11 Molecular dynamics results for the probability density for diffusion of particles of one species in a two-component, soft-sphere fluid at temperatures in the supercooled region. Results are shown for three different values of the reduced time $t^* = t/\tau$. Full curves: $t^* = 100$; dashes: $t^* = 300$; chain curves: $t^* = 500$. For argon-like values of the potential parameters and particle masses, $\tau \approx 2$ps; σ is an averaged size parameter. From J.L. Barrat et al., 'Diffusion, viscosity and structural slowing down in soft-sphere alloys near the kinetic glass transition', *Chem. Phys.* **149**, 197–208 (1990), *with permission of Elsevier.*

than 6%. Thus the diffusion mechanism changes very rapidly from one that is hydrodynamic-like to one consisting of a succession of activated jumps. Further strong evidence of the change in diffusion mechanism is provided by increasing deviations from the Stokes-Einstein relation (7.3.19) as the temperature falls below T_C; the diffusion coefficient D is found to be substantially larger than predicted, by orders of magnitude at the lowest temperatures explored in simulations[32] or experiments.[33] This trend is indicative of an increased decoupling of the single-particle motion from collective, viscous flow.

The pronounced slowing down of single-particle motion as a threshold temperature is reached is also visible in the behaviour of the self intermediate scattering function $F_s(k,t)$ defined by (7.5.12) or, equivalently, by

$$F_s(k,t) = \frac{1}{N}\sum_{i=1}^{N}\left\langle \exp\left(i\mathbf{k}.[\mathbf{r}_i(t) - \mathbf{r}_i(0)]\right)\right\rangle \tag{8.8.2}$$

Some molecular dynamics results[34] obtained for a binary Lennard-Jones (the Kob–Andersen model) are shown in Figure 8.12. (Note that time is plotted on a logarithmic scale.) At high temperatures the correlation function relaxes

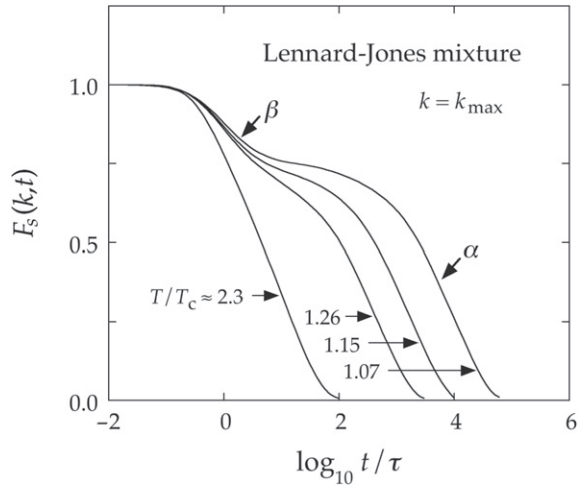

FIGURE 8.12 Molecular dynamics results for the self intermediate scattering function for particles of one species in a two-component Lennard-Jones fluid at temperatures in the supercooled region; k_{max} is the wavenumber corresponding to the main peak in the static structure factor. The labels α, β mark the two different relaxation regimes discussed in the text. For argon-like values of the potential parameters and particle masses, the unit of time is $\tau \approx 0.3$ ps. *Redrawn with permission from Ref. 34 © 1995 American Physical Society.*

to zero in near-exponential fashion. However, as the temperature is lowered into the supercooled region, the decay becomes very much slower and its exponential character is lost. As T approaches T_C, the relaxation proceeds in two, increasingly well-separated steps. After a fast initial decay on the time-scale of an inverse Einstein frequency, a first step (β-relaxation) leads to a plateau, where the function remains almost constant over two or more decades in time. The plateau is followed by a second step (α-relaxation) in which the correlation function finally decays to zero. The width of the plateau increases rapidly as the temperature is reduced. Eventually, when the temperature is sufficiently low, α-relaxation can be expected to set in only at times longer than those accessible in a simulation. The correlation function will then appear to level off at a non-zero value, signalling the onset of non-ergodic behaviour, at least on the nanosecond time scale of the simulation. The plateau value varies with k, but the general pattern seen in Figure 8.12 remains much the same over a wide range of molecular-scale wavenumber.

The decay of collective density fluctuations, as described by the full intermediate scattering function $F(k,t)$ (7.4.20) and measurable either experimentally or by simulation, shows a qualitatively similar behaviour to that of the single-particle function. The plateau value of $F(k,t)$ is analogous to the Debye–Waller factor of a solid; it provides a measure of the degree of structural arrest in the fluid, which persists for times that increase rapidly with

decreasing temperature. Over a temperature range just above T_C, the decay of either function in the α-relaxation regime, normalised by its value at $t = 0$, is accurately represented by a function of the form

$$f(t) = f_k \Phi\left(t^*\right) \tag{8.8.3}$$

where f_k is the plateau value, $t^* \equiv t/\tau_k(T)$ and $\Phi(t^*)$ is a universal scaling function. The wavenumber and temperature dependence of the decay enter only through the relaxation time $\tau_k(T)$ and the correlation functions are said to satisfy a time-temperature superposition principle. The scaling function is distinctly non-exponential, but is generally well-approximated by a Kohlrausch, stretched-exponential function, i.e.

$$\Phi(t^*) \approx \exp\left[-(t^*)^\beta\right] \tag{8.8.4}$$

where the exponent[35] β (<1 for stretching) is material and wavenumber dependent but independent of temperature.[36] Stretched-exponential behaviour is typical of relaxation processes in which the experimentally observed rate is determined by a wide distribution of relaxation times.

At temperatures below that of the kinetic glass transition the viscosity of the liquid increases dramatically, particularly in the case of fragile glass formers, meaning that the time required for the system to come to equilibrium after some perturbation is applied becomes much longer as the temperature decreases towards T_G. On realistic time scales the system falls out of equilibrium and equilibrium statistical mechanics no longer applies, a situation accompanied by the appearance of phenomena such as ageing, deviations from the fluctuation–dissipation theorem and spatial inhomogeneities in the particle dynamics.

The ageing of glassy materials is seen most obviously in the fact that their macroscopic properties usually change with time; for example, the molar volume of many polymeric glasses slowly decreases from the time of their preparation. On a microscopic level the ageing of supercooled liquids is reflected in the loss of time translational invariance even at temperatures above T_G. Time dependent correlation functions, as defined by (7.1.1), are now functions of two time arguments, t' and t'', not merely of the time difference $t = t' - t''$. An out-of-equilibrium system retains a memory of its initial state at a time t'', and its subsequent time evolution depends explicitly on both t' and t''. Let us suppose that a system in thermal equilibrium at a temperature above T_C at time $t = 0$ is quenched to a temperature $T \approx T_G$. The subsequent relaxation of the quenched system can be probed, after some waiting period t_0, by measurement of a time autocorrelation function of the form

$$C_{AA}(t_0 + t, t_0) = \left\langle A(t_0 + t)A^*(t_0)\right\rangle \tag{8.8.5}$$

where the statistical average is taken over equilibrium configurations at the initial temperature. It is found that the decay of the correlation function

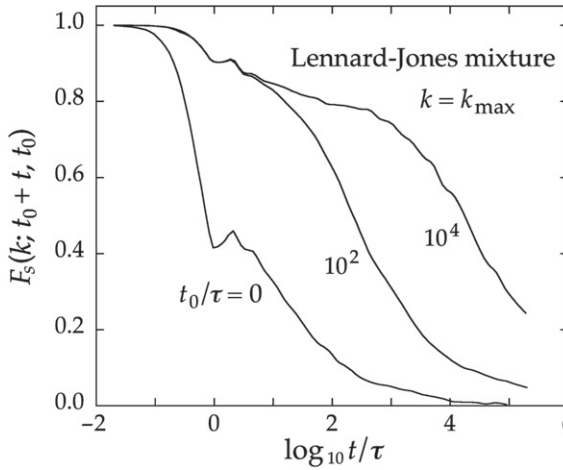

FIGURE 8.13 Decay of the self intermediate scattering function of a quenched Lennard-Jones mixture at a reduced temperature $T/T_C \approx 0.92$ for three values of the waiting time t_0 following the quench. For argon-like values of the potential parameters and particle masses the unit of time is $\tau \approx 0.3$ ps; k_{max} is the wavenumber corresponding to the main peak in the structure factor. *Redrawn from Ref. 37 with permission of European Physics Journal B © 2000 Springer.*

invariably slows down as the waiting time t_0 increases. An example taken from simulations of the Kob–Andersen model is shown in Figure 8.13, where the correlation function is again the self intermediate scattering function, $F_s(k; t_0+t, t_0)$, now defined in terms of the waiting time. Immediately following the quench, i.e. for $t_0 = 0$, the correlation function decays rapidly, but the rate of decay gradually reduces as t_0 increases. Data from both experiment and simulation, as well as theoretical considerations, suggest that at long times the autocorrelation functions of ageing systems satisfy a time/ageing-time superposition principle[37,38] of the form

$$C_{AA}(t_0 + t, t_0) \approx C^{\mathrm{s}}_{AA}(t) + C^{\mathrm{a}}_{AA}\left(\frac{h(t_0 + t)}{h(t_0)}\right) \tag{8.8.6}$$

The short-time contribution (superscript s) depends only on the time difference t, while the ageing part (superscript a) depends on the ratio $h(t_0 + t)/h(t_0)$, where $h(t)$ is a time-scaling function. In the case illustrated by Figure 8.13 the results at long times fall on a single curve if the scaling function is taken as $h(t) \propto t^{\alpha}$, with $\alpha \approx 0.88$.

Another feature of out-of-equilibrium systems, which is closely related to ageing, is the violation of the fluctuation-dissipation theorem. If the assumption of time translation invariance is dropped, the expression for the after-effect function in (7.6.13) becomes

$$\Phi_{BA}(t', t'') = \beta \left\langle B(t')\dot{A}(t'')\right\rangle = \beta \frac{\partial}{\partial t''} C_{BA}(t', t'') = \frac{\delta \left\langle \Delta B(t')\right\rangle}{\delta \mathcal{F}(t'')} \tag{8.8.7}$$

where the last equality follows from (7.6.12). The integrated response or susceptibility is then

$$\chi_{BA}(t',t'') = \int_{t''}^{t'} \Phi_{BA}(t',s)\mathrm{d}s = \beta \int_{t''}^{t'} \frac{\partial}{\partial s} C_{BA}(t',s)\mathrm{d}s$$
$$= \beta \left[C_{BA}(t',t') - C_{BA}(t',t'') \right] \tag{8.8.8}$$

For a system at equilibrium, (8.8.8) (with $t = t' - t''$) reduces to

$$\chi_{BA}^{\mathrm{eq}}(t) = \beta \left[C_{BA}(0) - C_{BA}(t) \right] \tag{8.8.9}$$

Thus, within the linear response regime, a parametric plot of $\chi_{BA}^{\mathrm{eq}}(t)$ versus $C_{AB}(t)$ yields a straight line of slope $-\beta$ irrespective of the choice of dynamical variables A and B. However, for systems far from equilibrium the fluctuation-dissipation theorem no longer holds. The non-equilibrium situation can be described by a generalisation of (7.6.13) having the form

$$\Phi(t',t'') = \beta\, \Psi(t',t'') \frac{\partial}{\partial t''} C(t',t'') \tag{8.8.10}$$

where we now restrict the discussion to autocorrelation functions but omit the subscript AA; in the case of time correlations described by (8.8.6), $t' \equiv t_0 + t$ and $t'' \equiv t_0$. The unknown function $\Psi(t',t'')$ is called the fluctuation-dissipation ratio. At equilibrium $\Psi(t',t'') = 1$ for all t',t''; away from equilibrium it is known[39] that within the mean field theory of spin glasses the fluctuation-dissipation ratio is a function only of the autocorrelation function to which it refers, i.e.$\Psi(t',t'') = \xi\left(C(t',t'')\right)$. It is generally assumed that the same simplifying property holds for structural glasses, for which the disorder is positional rather than magnetic. If that is so, then in its application to ageing (8.8.10) may be rewritten as

$$\Phi(t_0 + t, t_0) = \beta\xi\left(C(t_0 + t, t_0)\right) \frac{\partial C(t_0 + t, t_0)}{\partial t_0} \tag{8.8.11}$$

and the integrated response, as defined in the first line of (8.8.8) is now

$$\chi(t_0 + t, t_0) = \beta \int_{t_0}^{t_0+t} \xi(C) \frac{\partial}{\partial s} C(t_0 + t, s)\mathrm{d}s = -\beta \int_{C(t_0+t,t_0)}^{1} \xi(C)\mathrm{d}C \tag{8.8.12}$$

provided the correlation function is normalised by its value at $t = t_0$.

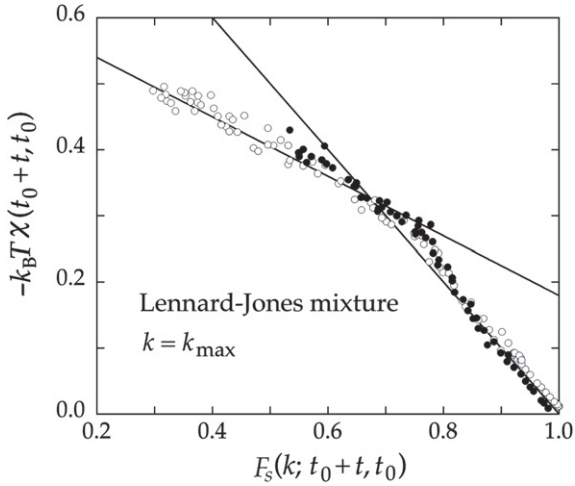

FIGURE 8.14 Parametric plot of susceptibility versus autocorrelation function for a supercooled Lennard-Jones mixture at two values of the waiting time t_0 and a reduced temperature $T^* = 0.3$. The dynamical variable involved is a Fourier component of the single-particle density. Open circles: $t_0/\tau = 1063$; closed circles; $t_0/\tau = 10^4$. For argon-like values of the potential parameters and particle masses the unit of time is $\tau \approx 0.3$ ps. See text for details. *Redrawn from Ref. 37 with permission of European Physics Journal B. © 2000 Springer.*

Examples of parametric plots of $\chi(C)$ versus C obtained by molecular dynamics calculations for the Kob–Andersen model at two values of the waiting time are shown in Figure 8.14. The correlation function in this case is again the self intermediate scattering function for a wavenumber corresponding to the main peak in the structure factor $S(k)$; the susceptibility measures the response of the system to a weak, external potential spatially modulated at the same wavenumber. The data are reasonably well fitted by two straight lines, with a clear break in slope when the correlation function has fallen to approximately 70% of its initial value. At short times the slope $p = -k_B T \mathrm{d}\chi/\mathrm{d}C \approx 1$, as it would be for a system at equilibrium, but at longer times $p \approx 0.45$; the fluctuation-dissipation theorem is satisfied at short but not at long times. The fact that the fluctuation-dissipation ratio at long times, ξ_∞, remains nearly constant as the correlation function decays to zero, i.e. as $t \to \infty$, suggests that relaxation in the long-time, ageing regime can be described in terms of an effective temperature

$$T_{\mathrm{eff}} = \frac{T}{\xi_\infty} > T \tag{8.8.13}$$

which depends on the temperature to which the system was quenched but is independent of t_0. Thus the rapidly relaxing modes of the glass, such as the 'rattling' motion of atoms in the cage formed by their nearest neighbours, respond to an external perturbation in a manner consistent with the equilibrium

fluctuation-dissipation theorem for the physical temperature T, while the slowly relaxing modes, associated with collective structural relaxation, are characterised by a higher, effective temperature T_{eff}. In these calculations ξ_∞ was found to be independent of wavenumber but more generally it appears to be independent of the choice of dynamical variable that the autocorrelation function monitors. The existence of a two-valued fluctuation-dissipation ratio is also apparent in studies of glassy systems driven into a stationary non-equilibrium state by the application of a steady, external force field.[40,41] In that situation, ageing is halted and time translation invariance restored, while the role of the waiting time t_0 in ageing glasses is played by the strength of the driving force. A good example is that of a sheared, supercooled fluid, where the rate of shear γ defines a time scale γ^{-1}. Molecular dynamics calculations[41] have confirmed that under such conditions the effective temperature for a given system and physical temperature is again independent of the dynamical variable which is probed.

A last example of the way in which the dynamics of strongly supercooled liquids differ from those of fully equilibrated systems is provided by a number of effects that are grouped together under the heading of *dynamical heterogeneity*. Whereas in equilibrium systems single-particle and collective motions are spatially homogeneous in the sense that they relax on the same time scale throughout the volume of the system, there is considerable evidence from both experiment[42] and simulation[43] of a high degree of spatial-temporal heterogeneity in supercooled liquids. Over time scales shorter than the structural relaxation time the system is a patchwork of active and quiescent domains.[44] In one type of domain, particle motions are coordinated; in the other, motion is primarily one of small amplitude vibrations around frozen positions. The active and quiescent states are intermittent, with the boundaries between the two domains evolving slowly with time. It has been conjectured[45] that the coexistence of active and quiescent regions may explain the observed, stretched-exponential behaviour that defines the α-relaxation regime. It has also been suggested that a growing and possibly divergent length scale of the domains might be associated with the divergence of the structural relaxation time as the temperature is reduced towards T_{G}; in the active domains, an increasingly large number of particles must move cooperatively to allow structural relaxation. The earliest simulations of binary mixtures identified the presence of highly correlated, string-like motions of adjacent particles, involving nearly instantaneous jumps over distances comparable with the interparticle spacing.[46] These observations were later confirmed by more extensive simulations[43] and by optical imaging studies of jammed, colloidal dispersions.[47] The coexistence near the kinetic glass transition temperature of two populations of particles that differ in their local dynamics is already visible in the probability densities pictured in Figure 8.8, a conclusion reinforced by numerical studies of the self part of the van Hove function for a variety of supercooled liquids.[48] For liquids at temperatures above T_{C}, $G_{\text{s}}(\mathbf{r}, t)$ is given

to a good approximation by the gaussian distribution (8.2.8). That result is a consequence of Fick's law (8.2.2), where the concept of a uniform diffusion coefficient is introduced. Below T_C a pronounced non-gaussian tail appears for displacements greater than roughly one particle diameter. The tail is well described by an exponential function of the form $G_s(r,t) \propto \exp[-r/\lambda(t)]$, where $\lambda(t)$ is a decay length that increases slowly with time. The picture that emerges is again one in which there are two populations of particles: those that are largely immobile and contribute to the central, gaussian part of the distribution; and those that are considerably more mobile and contribute to the exponential tail. Only at very long times is Fick's law behaviour recovered. A non-gaussian tail was also detected in the optical imaging experiments.

8.9 FLOW OF LIQUIDS AT THE INTERFACE WITH A SOLID

The static structure, interfacial thermodynamics and phase behaviour of confined, inhomogeneous fluids are by now well understood within the unifying framework of density functional theory, as described in Chapter 6. Significant progress has also been made in the experimental and theoretical investigation of dynamical processes at interfaces, stimulated in part by the increasing importance of nanofluidics and its technological applications.[49] In this section we show how the concepts and methods developed for the study of dynamics and transport in bulk liquids can be adapted to the flow of liquids close to a solid surface or confined to a narrow slit. On a macroscopic scale the flow pattern of a newtonian fluid, for which the local stress and strain rate are linearly related, is obtained by solution of the Navier–Stokes equation (8.3.16) subject to appropriate boundary conditions at any confining surfaces. An example is provided by Stokes's law (7.3.18). This gives an expression for the frictional force exerted by a flowing fluid on a suspended sphere in terms of a friction coefficient ξ, the value of which depends on the choice of boundary condition, stick or slip. The stick boundary condition is the one more appropriate for a sphere of diameter typical of large, colloidal particles. The situation on shorter length scales is more complex.

We take as an example the problem of fluid flow along a solid surface lying parallel to the xy-plane. Friction arises from the transfer of momentum from fluid to solid. If the surface is sufficiently rough, the assumption can be made that the tangential component of the local velocity field $\mathbf{u}(\mathbf{r},t)$ vanishes at the interface. This corresponds to the stick or 'no slip' boundary condition, which is the one commonly assumed to apply at the interface of a fluid with a macroscopic surface. In the case of an ideal, atomistically smooth surface there can be no transfer of momentum parallel to the surface; hence there is no frictional force and the slip boundary condition applies. Between these two extremes there will be situations of 'partial' slip, where the tangential component of velocity at the interface is non-zero, though usually small. For the sake of simplicity

we restrict the discussion to the case of laminar flow directed along the x-axis. Then the three possibilities we have listed can be accommodated within a single, phenomenological, boundary condition of the form[50]

$$\left(\frac{\partial u_x(z,t)}{\partial z}\right)_{z=z_h} = \frac{1}{b}u_x(z_h,t) \tag{8.9.1}$$

where b is the *slipping length*. Equation (8.9.1) applies at the 'hydrodynamic' boundary, positioned at $z = z_h$, which will not in general coincide with the surface of the solid. The value of z_h appears instead as a parameter of the theory sketched below; typically the hydrodynamic boundary is found to lie above the physical interface by one to two particle diameters.[51]

The three different scenarios consistent with (8.9.1) are represented by the Couette flow patterns pictured schematically in Figure 8.15. Part (a) of the figure corresponds to the stick boundary condition; the fluid velocity vanishes at $z = z_h$ and $b = 0$. For moderate degrees of roughness, but depending also on other features of the fluid-solid interaction, some 'velocity slip' may occur, as shown in part (b); this effect is measured by the *slip velocity*, $u_S = u_x(z_h)$. We shall see later that b is the distance below the hydrodynamic boundary at which u_x vanishes when the flow profile is extrapolated linearly into the solid. Part (c) corresponds to the limiting case of a perfectly smooth surface, where $b \to \infty$.

The quantity $\partial u_x/\partial z$ is the xz-component of the rate-of-strain tensor $\dot{\boldsymbol{\gamma}}$. Equation (8.9.1) may therefore be written as

$$\dot{\gamma}^{xz} = \frac{\partial u_x}{\partial z} \equiv \dot{\gamma} \tag{8.9.2}$$

where $\dot{\gamma}$ is the shear rate, which in turn is related to the xz-component of the stress tensor and shear viscosity of the bulk fluid by the constitutive relation (8.3.15):

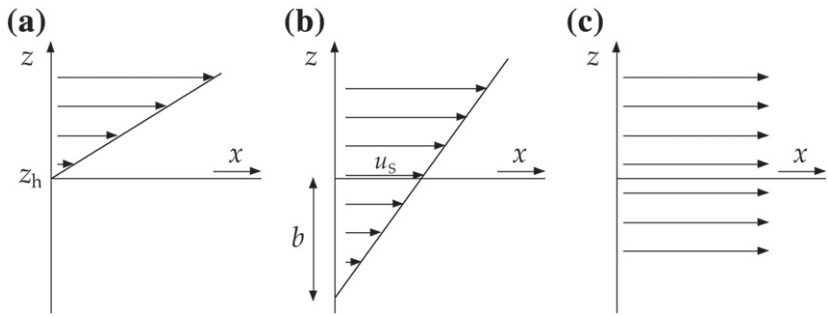

FIGURE 8.15 Schematic Couette flow patterns corresponding to (a) stick, (b) partial slip and (c) perfect slip boundary conditions, each applied at the hydrodynamic boundary $z = z_h$. In part (b), b is the slipping length and u_S is the slip velocity, i.e. the x-component of the fluid velocity field at $z = z_h$.

$$\Pi^{xz} = -\eta\dot{\gamma} \tag{8.9.3}$$

The stress tensor is also related to the tangential force F_λ exerted by the solid on the moving fluid:

$$\Pi^{xz} = -\lambda u_S = F_\lambda/\mathcal{A} \tag{8.9.4}$$

where $\mathcal{A}$ is the total surface area and λ is the fluid-solid friction coefficient. As $z \to z_h$, the internal friction (8.9.3) of the liquid must balance the friction (8.9.4) exerted by the wall, which implies that $u_S = (\eta/\lambda)\dot{\gamma}$. It then follows from (8.9.1) that the slipping length is given by the ratio of two transport coefficients:

$$b = \eta/\lambda \tag{8.9.5}$$

This result implies that the slipping length is an intrinsic property of a fluid at a given interface. It also shows that as the friction coefficient increases, b will decrease, and the boundary condition will become more and more stick-like. The two parameters that specify the boundary condition are b and z_h or, equivalently, for a fluid of given shear viscosity, λ and z_h. As we shall see, both λ and z_h are expressible in terms of microscopic dynamical variables[51], leading to Green–Kubo relations similar in nature to those that determine the transport coefficients of bulk fluids.

The hamiltonian of the fluid will contain the usual terms corresponding to interaction between particles of the fluid and that between fluid and solid, while the roughness of the surface can be represented by a periodic modulation of the fluid-solid potential. To complete a microscopic model of the system a stationary, Couette flow field $u_x(\mathbf{r})$ is imposed on the fluid by borrowing an idea used in non-equilibrium molecular dynamics calculations. A fictitious, non-newtonian, perturbation term $\mathcal{H}'$ is added to the unperturbed hamiltonian $\mathcal{H}_0$, where

$$\mathcal{H}' = \dot{\gamma}\sum_{i=1}^{N}(z_i - z_0)p_{xi} \equiv -\dot{\gamma}A \tag{8.9.6}$$

which also acts as the definition of a dynamical variable A. The x-component of the flow field induced by the perturbation is

$$\begin{aligned}\rho^{(1)}(\mathbf{r})u_x(\mathbf{r}) &= \left\langle \sum_{i=1}^{N} v_{xi}\delta(\mathbf{r}_i - \mathbf{r})\right\rangle \\ &= \frac{\int \exp\left[-\beta\left(\mathcal{H}_0 + \mathcal{H}'\right)\right]\sum_{i=1}^{N} v_{xi}\delta(\mathbf{r}_i - \mathbf{r})\mathrm{d}\mathbf{r}^N\mathrm{d}\mathbf{p}^N}{\int \exp\left[-\beta\left(\mathcal{H}_0 + \mathcal{H}'\right)\right]\mathrm{d}\mathbf{r}^N\mathrm{d}\mathbf{p}^N}\end{aligned} \tag{8.9.7}$$

where $\rho^{(1)}(\mathbf{r})$ is the single-particle density (2.5.11). Linearisation of (8.9.7) with respect to $\mathcal{H}'$, and use of the fact that both $\mathcal{H}'$ and the dynamical variable

to be averaged are odd functions of the particle momenta, shows that

$$\begin{aligned}\rho^{(1)}(\mathbf{r})u_x(\mathbf{r}) &= \beta m\dot{\gamma}\left\langle \sum_i v_{xi}(z_i - z_0)\sum_j v_{xj}\delta(\mathbf{r}_j - \mathbf{r})\right\rangle_0 \\ &= \dot{\gamma}(z - z_0)\left\langle \sum_i \delta(\mathbf{r}_i - \mathbf{r})\right\rangle_0 \\ &= \dot{\gamma}(z - z_0)\rho^{(1)}(\mathbf{r}) \end{aligned} \tag{8.9.8}$$

In the planar geometry assumed here, both $\rho^{(1)}(\mathbf{r})$ and $u_x(\mathbf{r})$ depend only on the coordinate z. The perturbation therefore gives rise to a velocity field of the required form:

$$u_x(z) = \dot{\gamma}(z - z_0) \tag{8.9.9}$$

which vanishes at $z = z_0$.

Let F_x^{s} be the instantaneous value of the force exerted by the solid on the moving fluid. Its mean value $\langle F_x^{\mathrm{s}}(t)\rangle$ at a time t can be calculated by the linear response theory of Section 7.6. From the general relations (7.6.12) and (7.6.13) we find that

$$\left\langle F_x^{\mathrm{s}}(t)\right\rangle = \beta\dot{\gamma}\int_0^t \left\langle F_x^{\mathrm{s}}(t - t')\dot{A}(0)\right\rangle_0 \mathrm{d}t' \tag{8.9.10}$$

where the average is taken over the unperturbed system, the dynamical variable A is that defined in (8.9.6), and the shear rate $\dot{\gamma}$ acts only from $t = 0$ and is thereafter constant in time. The time derivative of A is

$$\dot{A} = \sum_{i=1}^{N}\left(\frac{p_{xi}p_{zi}}{m} + (z_i - z_0)F_{xi}\right) \tag{8.9.11}$$

where $F_{xi} = F_{xi}^{\mathrm{f}} + F_{xi}^{\mathrm{s}}$ is the x-component of the total force acting on particle i; this is the sum of the microscopic forces due to other fluid particles (f) and the force arising from its interaction with the solid. From the definition (8.4.14) of the microscopic stress tensor in the $k \to 0$ limit, together with Newton's Third Law, which implies that $\sum_i F_{xi}^{\mathrm{f}} = 0$, it follows that (8.9.11) may be rewritten as

$$\dot{A} = \Pi^{xz} - z_0\sum_i F_{xi}^{\mathrm{s}} = \Pi^{xz} - z_0 F_x^{\mathrm{s}} \tag{8.9.12}$$

By substituting (8.9.12) in (8.9.10) and taking the limit $t \to \infty$, we obtain an expression for the total frictional force F_λ:

$$\begin{aligned} F_\lambda &= \lim_{t\to\infty}\left\langle F_x^{\mathrm{s}}(t)\right\rangle \\ &= -\beta\dot{\gamma}z_0\int_0^\infty \left\langle F_x^{\mathrm{s}}(t)F_x^{\mathrm{s}}(0)\right\rangle_0 \mathrm{d}t + \beta\dot{\gamma}\int_0^\infty \left\langle F_x^{\mathrm{s}}(t)\Pi^{xz}(0)\right\rangle_0 \mathrm{d}t \end{aligned} \tag{8.9.13}$$

If we take as definitions of the two quantities λ and z_h:

$$\lambda = \frac{\beta}{\mathcal{A}} \int_0^\infty \left\langle F_x^s(t) F_x^s(0) \right\rangle_0 \mathrm{d}t \tag{8.9.14}$$

and

$$z_h = \frac{\int_0^\infty \left\langle F_x^s(t) \Pi^{xz}(0) \right\rangle_0 \mathrm{d}t}{\int_0^\infty \left\langle F_x^s(t) F_x^s(0) \right\rangle_0 \mathrm{d}t} \tag{8.9.15}$$

the frictional force per unit area is

$$F_\lambda / \mathcal{A} = \dot{\gamma} \lambda (z_h - z_0) = -\lambda u_s \tag{8.9.16}$$

Identification of (8.9.16) with the phenomenological relation (8.9.4) shows that (8.9.14) and (8.9.15) represent Green–Kubo formulae for the friction coefficient and location of the hydrodynamic boundary, respectively, while (8.9.1), (8.9.9) and (8.9.16) together show that the slipping length b is given by

$$b = |z_0 - z_h| \tag{8.9.17}$$

where the boundary condition (8.9.1) is applied at $z = z_h$, with z_h determined by (8.9.15). Equivalently, given (8.9.5), b is determined by λ and η as evaluated from (8.9.14) and (8.4.20), and is therefore independent of the initial choice of z_0; a shift in z_0 leads only to a compensating shift in z_h. The expression for λ is analogous to that given for the friction coefficient ξ of Langevin theory by (7.3.8). Note, however, that whereas ξ is simply a frequency the dimensions of λ show that its meaning is that of momentum transfer per unit area per unit time.

Given a microscopic model of the fluid and surface, the correlation function expressions (8.9.14) and (8.9.15) can in principle be used to determine λ and z_h by equilibrium molecular dynamics simulation of a fluid confined between two parallel, planar surfaces. A less direct but more accurate method involves the computation of the transverse momentum density autocorrelation function $C_t(z, z'; t)$ of the confined fluid. The results of the simulation are then fitted to those obtained by analytical solution of the Navier–Stokes equation, similar to that of its **k**-space equivalent (8.4.2) in the bulk and based on the assumption that the boundary condition (8.9.1) applies at each surface; if the surfaces are identical, the fitting parameters are λ and b. The value thereby obtained for the slipping length is sensitive to the nature of the fluid-solid potential. If the interaction is strongly attractive, corresponding to a regime in which the liquid wets the surface, b is very small and the slip velocity $u_s \approx 0$. If the attraction is weak, b can become very large, of the order of tens of particle diameters, and 'near slip' boundary conditions apply.[52] Support for these conclusions has come experimentally from surface force measurements. In one investigation,[53] for example, a study was made of the flow behaviour of two, contrasting liquids, water and dodecane ($C_{12}H_{26}$), confined by hydrophilic or hydrophobic surfaces.

The stick boundary condition was found to apply for dodecane at both types of surface and for water at a hydrophilic surface. By contrast, in the hydrophobic case, where water does not wet the surface, a high degree of slip was observed, with $b \approx 19$ nm; this is some sixty times larger than the dimensions of a water molecule. The same experiments also showed that confinement had no measurable effect on the shear viscosity of either liquid down to film thicknesses of about 4 nm for dodecane and 10 nm for water.

REFERENCES

[1] Rahman, A., *Phys. Rev*. **136** A405 (1964).

[2] Landau, L.D. and Lifshitz, E.M.,'Fluid Mechanics', 2nd edn. Butterworth-Heinemann, Oxford, 1987, p. 44.

[3] Reif, F., 'Fundamentals of Statistical and Thermal Physics'. McGraw-Hill, New York, 1965, p. 168.

[4] (a) Mountain, R.D., *Rev. Mod. Phys*. **38**, 205 (1966). (b) Berne, B.J. and Pecora, R., 'Dynamic Light Scattering'. John Wiley, New York, 1976.

[5] Chapman, S. and Cowling, T.G., 'The Mathematical Theory of Non-Uniform Gases', 3rd edn. Cambridge University Press, Cambridge, 1970, p. 308. For a simplified discussion of the Boltzmann and Enskog equations see, e.g., Reed, T.M. and Gubbins, K.E., 'Applied Statistical Mechanics'. McGraw-Hill, New York, 1973.

[6] Heyes, D.M., *J. Phys. Condens. Matter* **19**, 376106 (2007), Table 1.

[7] Heyes, D.M., Cass, M.J., Powles, J.G. and Evans, W.A.B., *J. Phys. Chem. B* **111**, 1455 (2007).

[8] Harris, K.R., *J. Chem. Phys*. **131**, 054503 (2009).

[9] This is not the same effect as the $t^{-3/2}$ tail referred to in Sections 8.6 and 8.8.

[10] Boon, J.P. and Yip, S., 'Molecular Hydrodynamics'. McGraw-Hill, New York, 1980, pp. 249–50.

[11] For inelastic X-ray scattering and references to other neutron scattering experiments on liquid metals see, Scopigno, T., Ruocco, G. and Sette, F., *Re. Mod. Phys*. **77**, 031205 (2002).

[12] Alley, W.E., Alder, B.J. and Yip, S., *Phys. Rev. A* **27**, 3174 (1983).

[13] Levesque, D., Verlet, L. and Kürkijarvi, J., *Phys. Rev. A* **27**, 1690 (1973).

[14] Bodensteiner, T., Morkel, C., Gläser, W. and Dorner, B., *Phys. Rev. A* **45**, 5709 (1992); erratum: *Phys. Rev. A* **46**, 3574 (1992).

[15] Sigurgeirsson, H. and Heyes, D.M., *Mol. Phys*. **101**, 469 (2003).

[16] Rahman, A., *In* 'Neutron Inelastic Scattering', vol.1. IAEA, Vienna, 1968.

[17] Jacucci, G. and McDonald, I.R., *Mol. Phys*. **39**, 515 (1980).

[18] Erpenbeck, J.J. and Wood, W.W., *J. Stat. Phys*. **24**, 455 (1981).

[19] Keyes, T. and Oppenheim, I., *Physica* **70**, 100 (1973).

[20] Evans, D.J., *Mol. Phys*. **47**, 1165 (1982).

[21] (a) Alley, W.E. and Alder, B.J., *Phys. Rev. A* **27**, 3158 (1983). (b) Kambayashi, S. and Kahl, G., *Phys. Rev. A* **46**, 3255 (1992).

[22] Schofield, P., *Proc. Phys. Soc*. **88** 149 (1966).

[23] (a) Alder, B.J. and Wainwright, T.E., *Phys. Rev. Lett*. **18**, 988 (1967). (b) Alder, B.J. and Wainwright, T.E., *Phys. Rev. A* **1**, 18 (1970).

[24] Pomeau, Y. and Résibois, P., *Phys. Rep*. **19**, 63 (1975).

[25] (a) Dorfman, J.R. and Cohen, E.G.D., *Phys. Rev. A* **6**, 776 (1972). (b) Dorfman, J.R. and Cohen, E.G.D., *Phys. Rev. A* **12**, 292 (1975).
[26] (a) Ernst, M.H., Hauge, E.H. and van Leeuwen, J.M.J., *Phys. Rev. A* **4**, 2055 (1971). (b) Erpenbeck. J.J. and Wood, W.W., *Phys. Rev. A* **26**, 1648 (1982).
[27] Levesque, D. and Ashurst, W.T., *Phys. Rev. Lett.* **33**, 277 (1974).
[28] The conclusions of Ref. 27 were later confirmed, with much higher precision, by simulations of a lattice-gas model for which the equations of motion can be solved exactly: see van der Hoef, M.A. and Frenkel, D., *Phys. Rev. A* **41**, 4277 (1990).
[29] Morkel, C., Gronemeyer, C., Gläser, W. and Bosse, J., *Phys. Rev. Lett.* **58**, 1873 (1987).
[30] This classification is due to Angell, C.A., *J. Phys. Chem. Solids* **49**, 863 (1988).
[31] Simulations of the glass transition are commonly carried out on mixed systems as a device to inhibit crystallisation.
[32] Barrat, J.L., Roux, J.N. and Hansen, J.P., *Chem. Phys.* **149**, 198 (1990).
[33] Mapes, M.K., Swallen, S.F. and Ediger, M.D., *J. Phys. Chem. B* **110**, 507 (2006).
[34] Kob, W. and Andersen, H.C., *Phys. Rev. E* **52**, 4134 (1995).
[35] The conventional use of β for the Kohlrausch exponent is unfortunate, since it refers to the decay in the α-relaxation regime.
[36] For an example of a fit of the Kohlrausch law to experimental data, see Wuttke, J., Petry, W. and Pouget, S., *J. Chem. Phys.* **105**, 5177 (1996).
[37] Kob, W. and Barrat, J.L., *Eur. Phys. J. B* **13**, 319 (2000).
[38] Berthier, L. and Biroli, G., *Rev. Mod. Phys.* **83**, 587 (2011).
[39] Cugliandolo, L.F. and Kurchan, J., *J. Phys. A* **27**, 5749 (1994).
[40] Cugliandolo, L.F., Kurchan, J. and Peliti, L., *Phys. Rev. E* **55**, 3898 (1997).
[41] Berthier, L. and Barrat, J.L., *J. Chem. Phys.* **116**, 6228 (2002).
[42] Ediger, M.D., *Ann. Rev. Phys. Chem.* **51**, 99 (2000).
[43] Glotzer, S.C., *J. Non-Cryst. Solids* **274**, 342 (2000).
[44] Figure 5 of Perera, D.N. and Harrowell, P., *J. Chem. Phys.* **111**, 5441 (1999).
[45] Berthier, L., Biroli, G., Bouchaud, J.P., Cipilletti, L., El Masri, D., L'Hôte, D.L., Ladieu, F. and Pierno, M., *Science* **310**, 1797 (2005).
[46] Miyagawa, H., Hiwatari, Y., Bernu, B. and Hansen, J.P., *J. Chem. Phys.* **88**, 3879 (1988).
[47] Weeks, E.R., Crocker, J.C., Levitt, A.C., Schofield, A. and Weitz, D.A., *Science* **287**, 627 (2000).
[48] (a) Chaudhuri, P., Berthier, L. and Kob, W., *Phys. Rev. Lett.* **99**, 060604 (2007). (b) Chaudhuri, P., Sastry, S. and Kob, W., *Phys. Rev. Lett.* **101**, 190601 (2008).
[49] Bocquet, L. and Charlaix, E., *Chem. Soc. Rev.* **39**, 1073 (2010).
[50] Bocquet, L. and Barrat, J.L., *Soft Matter* **3**, 685 (2007).
[51] Bocquet, L. and Barrat, J.L., *Phys. Rev. E* **49**, 3079 (1994).
[52] Barrat, J.L. and Bocquet, L., *Faraday Disc.* **112**, 119 (1999).
[53] Cottin-Bizonne, C., Cross, B., Steinberger, A. and Charlaix, E., *Phys. Rev. Lett.* **94**, 056102 (2005).